TRW TPF Architecture
Phase 1 Study,
Phase 2 Final Report

Table of Contents

1   Phase I

1.1   Intro: Goal of the first phase/selection of architectures

The team sections shown here are the writeups of Phase I specified in the contract.

1.2   TRW Phase I Study

1.2.1   Approach

During Phase I, TRW performed an objective trade study on a variety of potential architectures that could conceivably do the TPF mission. When we started the study, we assumed the field was wide open with the evaluation process used to eliminate those concepts which were not feasible in the TPF mission timeframe, even with significant technology development funding. We put together a very diverse science team to bring different areas of expertise to work on the problem. We found five categories of architectures that fell into two classes, Direct Imaging systems (DIs) and Synthetic Imaging systems (SIs). Given a normalized detection and characterization performance, we found DIs to have some advantages over SIs as presented below.

In this section we describe our team and its organization, the requirements the team worked to in Phase I, the processes we developed for looking at the architectures, and the metrics used for evaluation.

1.2.1.1 Team organization

Our Phase I team is shown in Figure X1-1. During this phase, the effort was lead by our science team with feasibility and small study support coming from the engineering team. The Systems Engineer led the effort to define the processes and metrics used for identifying and evaluating the concepts as proposed by the science team. A significant effort on mirror manufacturing issues was performed by our Kodak teammates.

Figure X1-1: TRW TPF Phase I Study Team			
INDUSTRY		**SCIENCE TEAM**	
Name	**Company/Role**	**Name**	**Organization**
Mark Abrams	ITT PM	Craig Copi	Case Western Reserve University
Charlie Bennett	LLNL	Vincent Coude du Foresto	DESPA, Meudon, FR
Arthur Buettner	Kodak Mech Engr	Alan Dressler	Carnegie Institute (Pasadena)
Mike Busby	Consultant	James Graham	UC Berkeley
Steve Cain	ITT	Tom Herbst	Science Team
Suzi Casement	TRW Science	Ken Johnston	US Naval Observatory
Doug Cohen	ITT	James Larkin	UCLA
Marty Flannery	TRW Payload	Liz Gire	Student (UCLA)
Brent Helleckson	SEE L2 orbit expert	Doug Lin	Lick Observatory
Richard Hertel	ITT	Bertrand Mennesson	Science Team (I/F)
Pete Jarecke	TRW Payload	Frank Shu	UC Berkeley
Peter Jones	Kodak Optical SE	Richard Simon	NRAO
Keith Kroening	TRW Payload Support	Glenn Starkman	Case Western Reserve University
Don Kwak	TRW Configuration	John Trauger	JPL
John Lesveaux	Kodak PM/Mech Eng	Steve Vogt	Lick Observatory
Ray Manning	TRW Dynamics	Dan Weedman	Self
Gary Matthews	Kodak	Ned Wright	UCLA
James McCarthey	TRW		
Stewart Moses	TRW System Engineer		
Jeff Nienberg	TRW Thermal		
Vinod Patel	Kodak Optical SE		
Bill Sharp	ITT		
Michael Wehner	TRW Program Manager		

1.2.1.2 Requirements

The TPF Mission requirements are listed in Exhibit II of the RFP. A subset of key requirements affecting feasibility were used as "gateway" requirements in Phase I which determined if a concept would be further pursued. In addition, 150 stellar targets had to be identified for the TPF mission. Realizing that the 150 closest F, G, & K stars would include some poor candidates due to variability, evolutionary status, etc., Dr.'s R. Simon and S. Vogt worked to develop a target list of good candidates. The process, which used the HIPPARCOS catalog as the starting point, is described in Simon & Vogt, 2000 (BAAS, **32**, p. 1485). Of the > 600 stars in the initial list, only 163 made the "Golden Oldies" list of good TPF candidates. The makeup of the Golden Oldies determined the angular separation, the contrast ratio, and the distance to which the TPF architecture would have to operate. Figure X1-2 lists the requirements from the PAR and as derived by TRW that were used to configure the concepts investigated.

Figure X1-2: Requirements Collected for PAR		
Parameter	**Requirement**	**Source**
Mission duration	5 year requirement; 10 year goal	RFP
Investigation allocation	50% Planet detection/characterization, 50% Astrophysics	RFP
Number of targets	At least 150 for detection, at least 20 for characterization	RFP
Detection criteria	SNR = 5	TRW
Angular threshold	50 milli-arcseconds	TRW
Sky coverage	4π steradian (goal; if less, must increase distance to targets)	TRW
Integration time	< 24 hours for detection; < 2 weeks for characterization	RFP/TRW
Wavelength range	VIS: 0.5 – 1.5 microns (TBR); IR: 7 - 17 microns	RFP/TRW
Spectral resolution	VIS: at least R = 100 (TBR); IR: at least R = 20	RFP/TRW
Characterization performance	SNR = 5 for spectral lines	TRW/SWG
Number of revisits	2 for detection, 7 total (including characterization)	SWG
Revisit frequency	Not less than 1 month	SWG

One key requirement to come out of our analysis is the estimate that a single detection observation will have to take less than 24 hours on average including all observing overhead. This is an average over all the observed systems which will have a very large spread of observing time requirements. However, it is a useful parameter to help size the architectures.

1.2.1.3 Concept Identification and Evaluation Process

The concept identification effort during Phase I was on-going throughout the study. The program kickoff for Phase I was a science team meeting that provided the majority of the ideas that were pursued. The process collected a large number of initial ideas which were then culled to provide a short list of candidates which could meet the TPF mission requirements. The first cut produced the identification of two categories for planet detection, direct and indirect, of which only direct detection methods were able to perform the TPF characterization mission. Direct detection can be done by either scattered (reflected) light or emitted light from the planet, leaving only the visible and thermal infrared as feasible wavelength regions to perform the TPF mission.

From the remaining candidates, we identified two broad classes of direct detection architectures: synthetic imaging which samples the UV plane sequentially, and direct imaging which simultaneously samples a large fraction of the UV plane. The ideal TPF would be a fully filled large aperture direct imager with sufficient angular resolution to fully separate the star from the planet. However, this concept was determined to be infeasible due to the cost of fabricating and launching such a system, even if the system could be designed to meet the required wavefront error requirements. That left the remaining trade space of smaller, more complex, or underfilled direct imagers, and a variety of synthetic aperture (or interferometer) approaches.

The process of determining whether to pursue a given concept included:
- Scientific merit of the observing scheme and capabilities provided by the concept
- Technical feasibility (using engineering judgement) for the TPF time scale
- Cost estimates on the TPF time scale

This process resulted in the concepts listed in Figure X1-3. This is by no means an exhaustive list as many of these techniques can be combined or used at other wavelengths. These however were the concepts that the TRW TPF team felt worthy of further evaluation.

Figure X1-3: TPF Phase I Concept List			
Architecture Name	**Abbreviation**	**Wavelength**	**Method for Addressing Contrast**
Nulling Interferometer (Monolith or Formation Flying)	NIM and NIFF	Thermal Infrared	Starlight suppressed through interferometric cancellation in either an attached monolithic structure or a set of formation flying apertures plus a beam combiner spacecraft.
Large Aperture with Coronagraph	LAC	Thermal Infrared	Starlight suppressed by apodized occulting spot in instrument optics
Free-flying Occulter	FFO	Visible	Starlight suppressed by occulting body external to telescope
Fresnel Lens	FL	Thermal Infrared	Operates as large aperture with coronagraph, but with transmitting instead of reflecting primary optics
Ultra-Large Sparse Aperture	ULSA	Visible to Near Infrared	Aperture sized sufficiently large to resolve planet and star, starlight suppressed with simple internal occulting spot

Once identified, these concepts were evaluated against the JPL Criteria using the evaluation flow shown in Figure X1-4. We used these criteria to develop an overall system utility function and used the results to rank each architecture against cost. We also evaluated the performance of each system against an analog of the Solar System placed at 10 pc. In the architecture descriptions in section x.2, observations of this system are described. The benchmark system is modeled using blackbody approximations for the Sun and for the planets in the case of the thermal infrared systems, and typical albedos and 50% illumination for the visible reflected light from the planets. The spectral models use the Earth spectra as provided in Phase I by the TPF SWG. The exo-solar zodiacal light contributions are modeled using a COBE model generated by Dr. Edward Wright based on COBE observations. In general, either a face on or a 45° view angle was used for the zodiacal cloud.
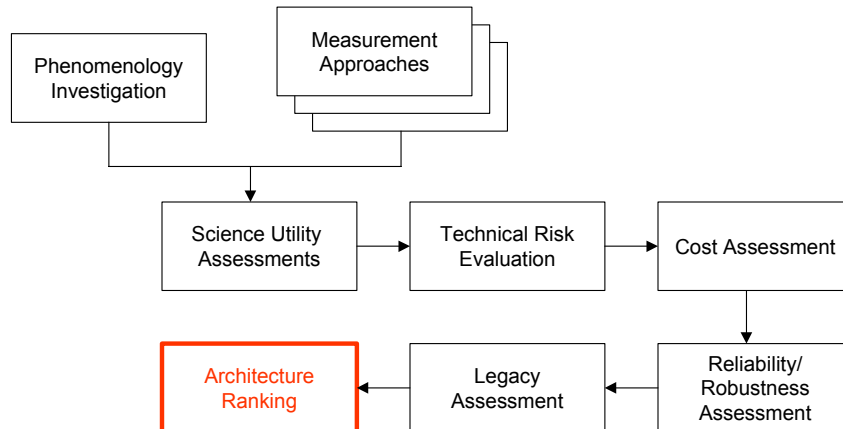

Figure X1-4: Architecture Evaluation Process

1.2.1.4 Metrics used for evaluation

Specific metrics were developed to derive a numeric value for a "system utility function" that was then ranked against the projected system cost. The system utility function has 4 parts, each of which has specific evaluation criteria that the TPF Phase I team used to rate each of the architecture concepts. Figure X1-5 lists the Science Utility and Technical Risk evaluation factors which were evaluated on a High, Medium, Low scale, with high = 3, medium = 2, and low = 1 point which were summed over the factors. For the science utility function, high was good, while for the technical risk function, low was good.

Figure X1-5: Overall System Utility Metrics for Science Utility and Technical Risk		
Factor	**Subfactor**	**Detailed Evaluation Criteria**
Science Utility Function Max poss. = 27 Min poss. = 9	Exo-planet Detection	Ability to determine orbit
		Ability to overcome confusion due to exo-zodi structure
		Ability to handle multiple planets viewed simultaneously
		Ability to handle high exo-zodi density

	Exo-planet Characterization	Ability to determine planet temperature
		Ability to determine atmospheric composition
	Other Astrophysics	Ability to image multiple point sources
		Ability to image extended, low-contrast targets
		Ability to perform general spectroscopy
Technical Risk Assessment Max poss. = 54 Min poss. = 13	Optics	Mirror material technology
		Mirror figure control
		Downstream optics
		Coronagraph technology
		Pathlength control
		Polarization control
		Beam intensity control / beam splitting
		Transmissive material technology
		Optics deployment technology
		Metrology
		Assembly in space
	Flight System technology	Thermal control
		Attitude control
		Alignment of optical elements
		Dynamics control
		Precision station keeping
		Formation initialization
		Deployable structures
		Operational complexity
		Pre-launch test complexity

The last two factors in the overall system utility function are evaluated slightly differently. The third factor, Reliability / Robustness, is determined by the degree of functional redundancy evaluated over all of the system elements of an architecture. The greater the number of system elements, particularly those for which a loss of one would end the mission, the lower the evaluation against this factor. To evaluate this, each architecture was divided into system elements (collecting optics, spacecraft, etc.) and characterized as to whether the loss of that element would end the mission, whether there was internal redundancy in that element, and whether or not the system could compensate for degradation in that element. A high risk element was one that can end the mission and cannot be made internally redundant (e.g. primary mirror optics). A moderate risk element was one that cannot be lost but can be made internally redundant (e.g. spacecraft electronics). The reliability / robustness evaluation counted the number of high risk and medium risk elements, using high = 3, medium =2 (0 for low risk items), to give a maximum value of 33 and a minimum value of 6 depending on the number of elements in the architecture.

For the last factor in the evaluation, the "legacy" to future missions that an architecture would provide, we only considered Planet Imager and Life Finder as direct follow-on missions to TPF. Obviously, the technology developed for TPF could have much wider utility, but these two missions are the direct decedent Origins missions that would like to use direct technology insertion if possible. To evaluate this factor, the technologies needed for planet imager and life finder were projected and the applicability of each of the architecture components was evaluated against those needs. Also evaluated was the ability for the architecture to "evolve" up to large scales or multiple systems. These systems were then evaluated for evolvability on the High, Medium, and Low scale, based on the applicability of the technologies in the architecture that would scale up or apply to Life Finder and Planet Imager. A maximum score of 6 was possible.

These 4 factors were then combined using a weighted ranking, scaling the points to be on the same scale:

System utility = science utility + legacy – (technical risk + reliability risk)

This evaluation weights science utility as 2/3, risk as 2/9 (1/9 for each of technical and reliability risk) and legacy as 1/9. This utility function is then evaluated against the system cost. The overall ranking and recommendations are discussed in section 1.x.3 below.

1.2.2 Concepts investigated

Our Phase I TPF study resulted in 6 architectures that met the basic mission requirements and were then more fully evaluated. These are the Free-Flying Nulling Interferometer (NIFF), the Monolithic Nulling Interferometer (NIM), the Large Aperture Coronagraph (LAC), the Fresnel Lens Coronagraph (FL), the Free-Flying Occulter (FFO), and the Ultra-Large Sparse Aperture (ULSA). A point design for all of these concepts was developed and evaluated against the evaluation criteria and specific metrics described above. This section describes the key features, performance characteristics, critical elements, and required technology development for each of the concepts.

1.2.2.1 IR Nulling Interferometer, Monolithic and Free Flying Configurations

The baseline TPF concept as presented in the TPF glossy book in 1999 was a free-flying nulling interferometer with 4 collecting apertures and a combiner spacecraft. Based on the amount of work that was done at that time, this was obviously a concept that could perform the TPF mission. For this study, we looked at a variety of configurations, including everything from a Bracewell pair to 2-D configurations with up to 10 collecting apertures. Based on modeling described below, a 1-3-3-1 linear array of apertures (the "OASES" configuration) produces a null of sufficient depth and width to perform the TPF mission. Increasing the number of apertures added complexity without significant increase of scientific capability, at least given the parameters we investigated in Phase I. Therefore, we took as our baseline configuration a 1-3-3-1 linear nulling interferometer. Further trades on system efficiency v. configuration were to be performed in Phase II.

There remained the trade between fixed apertures on a large precision structure utilizing flight proven deployment technologies (monolithic, NIM) and 5 free-flying spacecraft where each aperture is its own spacecraft with an additional spacecraft for the beam combiner (NIFF). The requirements and capabilities of these options were considered sufficiently different to include both in the detailed evaluation process of Phase I. The performance characteristics of these two configurations are nearly identical but the technology development needs and the additional astrophysics they can do are quite different. In addition, the NIFF configuration offers the capability of tuning the spacecraft separation and therefore the null width to the characteristics of the stellar system being observed. However, the configuration selection also affects requirements such as fuel, cooling, flight control, mass, and launch vehicles, which were also investigated as part of the Phase I study.

In this section we present the baseline configuration, the results of the modeling that led us to select the OASES configuration as our baseline, the sensitivity analysis that led to the development of the technology drivers for these configurations, the performance of the baseline configuration for planet detection, and a novel concept for improving the detection capabilities which also allows the removal of some systematic errors. Finally, we discuss the technology development required to achieve either of the configurations discussed.
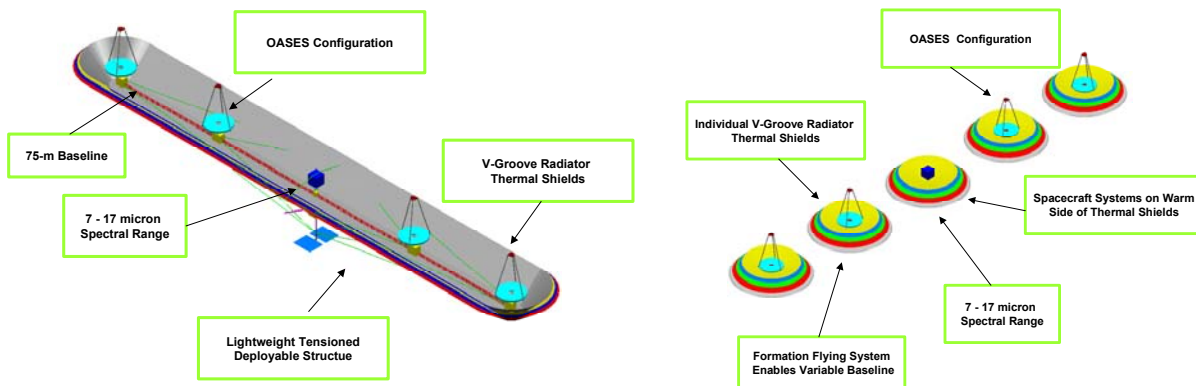
1.2.2.1.1   Baseline Configurations

Figure X2-1: Baseline configurations for the NIM and NIFF architectures.

Figure X2-1 shows each of the NIM and NIFF configurations used in the Phase I evaluation process. Detailed discussion of the various configurations considered was presented at the PAR. For the study, the diameter of the

apertures was 2.5 m for the inner two and 0.8m for the outer two. This was sufficient for the detection of Earth around the sun at 10 pc without driving mirror manufacture. Obviously the configurations have limitations on the available sky coverage to maintain the needed cold temperatures for the thermal IR observations. Other options were considered and are discussed in the PAR presentation.

1.2.2.1.2   System Models and Performance

Nulling interferometry offers the ability to achieve very high spatial resolution and suppression of the central star with relatively small individual telescopes. But interferometery, especially when used for nulling, requires extremely delicate control of mirror surfaces, spacecraft positioning, phase delays, pointing and beam matching. As part of our architecture review, we analyzed a wide variety of interferometer patterns and the fragility of the central null. In order to investigate interferometer geometries and effects that impact the null, we produced an interferometer simulator. An arbitrary number of telescopes can be simulated with 1-D and 2-D geometries and with variable phase and a wide range of error terms. For each geometry, errors are added stochastically and a large number of realizations are produced so that not only the level of the null but also the variation of the null can be investigated. These variations are as important as the overall null level because they represent fluctuations of the measured intensity that must be rejected. To allow us to model effects such as high order wavefront error and optical coating variations, each telescope is broken into 36 individual apertures. This also allows the natural beam attenuation to come out naturally in the analysis. The null is evaluated by integrating the central region of the interferometer pattern over a circular stellar disk in which the disk is assumed to be of constant brightness.

Several architectures were analyzed ranging from simple Bracewell 2-element arrays, up to 10 element Mariotti arrays. In general the more elements within the array, the wider the null produced with some exceptions. Arrays with more elements, however, are more sensitive to errors in that their wider null depends more critically on balancing many aspects of the interferometer pattern. In general, any of the 4-element linear interferometers (OASES) produces a sufficiently wide null to satisfy the planet finding requirements. There is very little difference in the signal or modulation efficiency of different arrays on the actual planet detection. By far the most important parameter is the nulling width. Given these results we selected the linear 1-(3-e)-(3-e)-1 OASES pattern, for detailed analysis of the fragility of the null.

Fragility of the central null
In a real interferometer a large number of errors can occur, but they can be subdivided into four main effects: relative beam attenuation, phase errors, station keeping errors of the spacecraft and pointing errors of individual telescopes. To model the cumulative errors, we systematically varied the rms level of these terms and calculated multiple versions of the same array. For each version the central null was integrated and plotted as the fraction of the
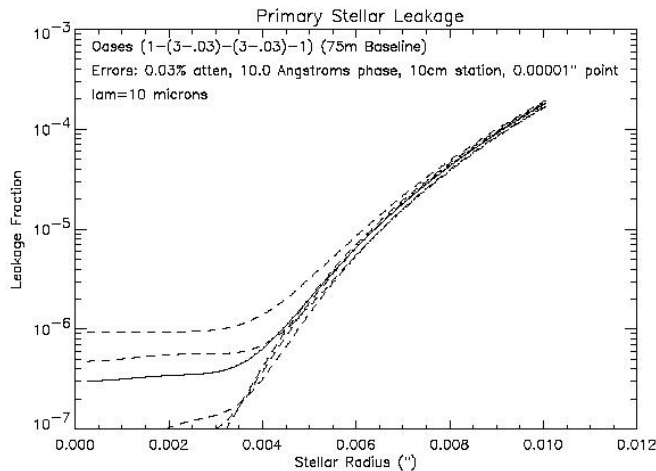

central star light that leaks into the detected emission against the radius of the star. The average leakage is also computed from all of the versions. Figure X2-2 shows the baseline configuration with relative attenuation errors of 0.03%, 10 Å of relative phase errors, 10 cm of spacecraft position error and 10 μarcsecond pointing errors. The average leakage is shown as the solid curve, with the dashed curves showing 4 different individual leakages. As one can see, the general result is that for a given version, the null depth is relatively flat at a level determined by the errors until the ideal quality of the null becomes worse than the error level. In this particular example, the average null out to a stellar radius of almost 4 milliarcseconds is 3×10^{-7}, while fluctuations as high as 1×10^{-6} occur a non-trivial amount of the time.

Figure X2-2: Stellar leakage v. radius for a set of errors.

For a typical TPF operational scenario, we looked at a 12 hour observation set with a desired rms starlight fluctuation under 10^{-8}. This requires an intensity imbalance between the four telescopes of less than 1.5×10^{-4}. If we evenly assign this error in quadrature between optical errors on individual optics, telescope mispointing, overall

phase errors and differential polarization we produce an error budget of: 12nm rms for optics (3nm rms for each of 19 optics), pointing errors of the inner Bracewell pair of 0.0034", pointing errors of outer Bracewell pair of 0.01", phase error of 28 nm (piston), relative polarization between beams of 1 degree. These errors will drive the technology development requirements in many areas.

Planet Detectability

Producing a deep, wide null is not necessarily sufficient to detect a planet. A terrestrial planet is not expected to be alone within the stellar system. Multiple planets as well as exo-zodiacal dust can significantly complicate the scene visibility. We used the same interferometer simulator to model the detected fluxes of the benchmark solar system analog. The left panel of Figure X2-3 shows the benchmark system viewed at 10 μm. The middle panel is the transmission pattern of a 1-3-3-1 OASES style interferometer at one orientation. The right panel is the net image produced. The interferometric signal is proportional to the integral of the right image. Figure X2-4 shows the signal from this simulated system as a function of interferometer orientation. At 10 μm, by far the largest signal is due to the exo-zodiacal background. The planets Venus and Mercury would each produce a signal greater than that of Earth due to their higher temperatures and because the interferometer beam is falling off with radius. In these simulations, the central star is assumed to be fully suppressed. The signal strengths of the planets and exo-zodi does not depend significantly on the errors in the interferometers, while the null depends critically on these terms.
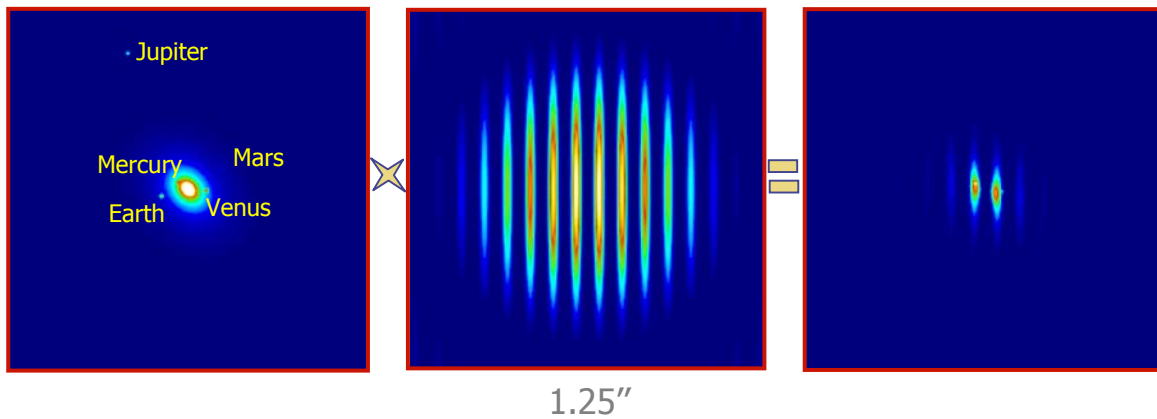

Figure X2-3: Model of the Solar System at 10 pc. Left panel is the input at 10 microns, middle panel is the response function of the baseline configuration, right panel is the resulting signal through the interferometer.
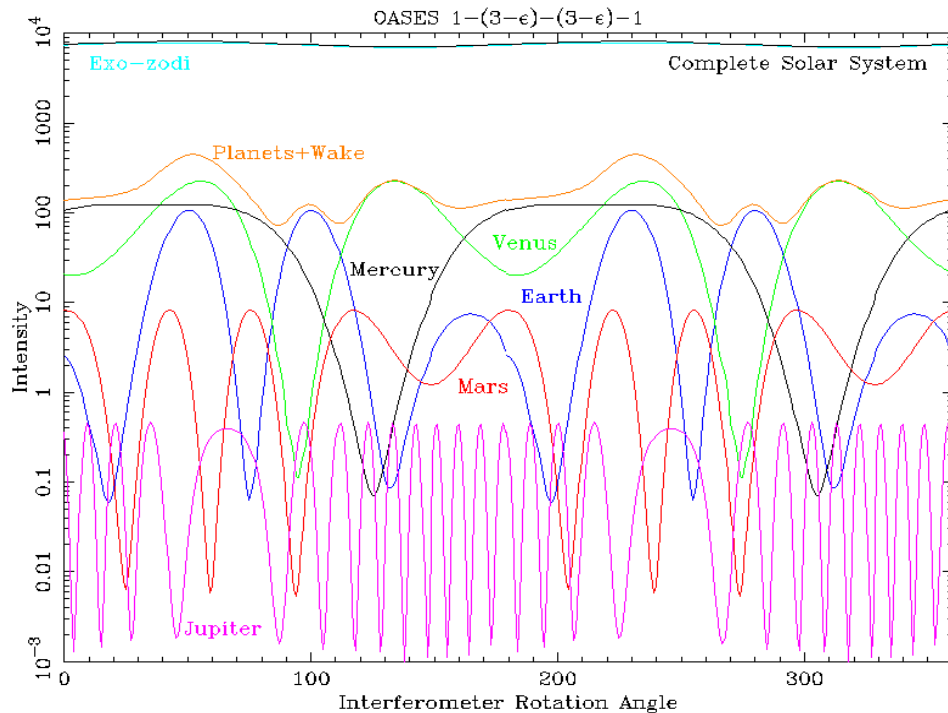

Figure X2-4: The signal response at 10 microns as a function of rotation angle for the solar system at 10 pc by component.

7

If the central null can be maintained at the levels necessary, an exo-zodiacal disk will still swamp the signal of any planet. One idea developed in Phase I that offers some improvement over simply staring with the interferometer is to nod the interferometer by a small amount (few tenths of an arcsecond). This nodding is done perpendicular to the alignment of the array, presumably using chopping secondaries or a tip-tilt mirror. There are several benefits to this procedure if it can be achieved while preserving the null. First, it gives a differential measurement at each interferometer angle removing some systematic effects such as slow changes in the pattern geometry, and variations in the local zodiacal background. Another benefit is that the beam efficiency falls off with radius and by chopping the beam symmetrically, we would place the peak efficiency on the planet and then off causing an improved relative signal for objects at roughly the separation that is equal to the chopping, while symmetric objects such as the exo-zodi and the central star itself will receive an additional level of nulling. The left panel of Figure X2-5 shows the intensity detected by the interferometer while staring and the right panel shows the effect of differential nodding. The exo-zodi is fully removed except for asymmetries due to the wakes of the planets. Planets with orbits both larger and smaller than the nod pattern are also partially suppressed as can be seen with Mercury and Jupiter. Planets with separations close to the nod size, such as the Earth and Venus, are only marginally suppressed by this nodding making them easier to detect. A final benefit of nodding is that even at a couple of interferometry angles, nodding will reveal if the system is asymmetric. This can quickly and efficiently give a first indication that a star is worth further investigation. Although this style of interferometry has never been attempted, we believe it should be investigated further if an interferometer is selected for further study.
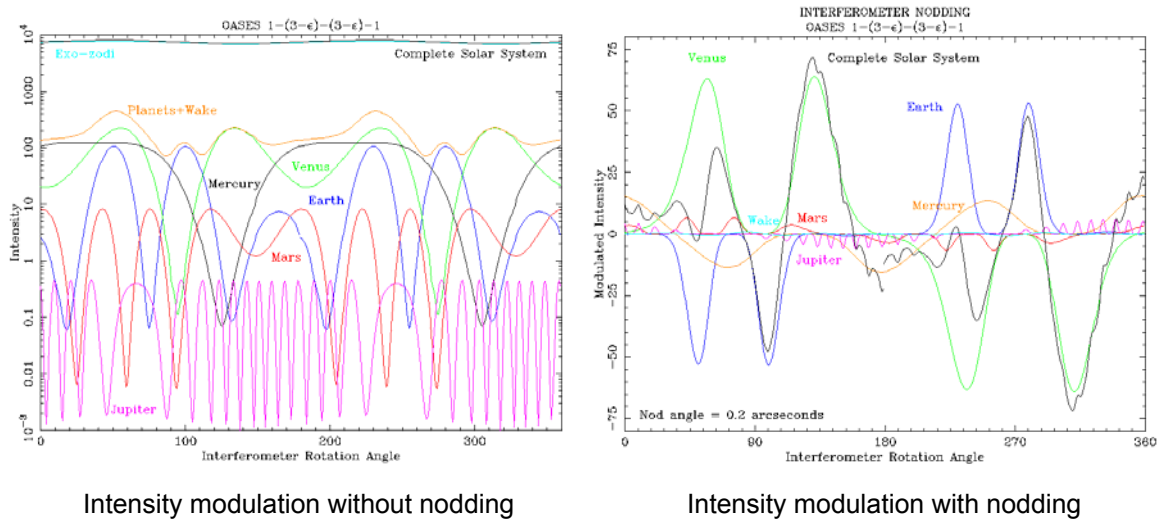

| Intensity modulation without nodding | Intensity modulation with nodding |

Figure X2-5: Significant improvement in planet detection may be realized by nodding the image along the null.

1.2.2.1.3   Spacecraft requirements

Regardless of interferometer geometry, the telescope array only samples one location in the UV plane at one time. So producing an image of a stellar system requires rotation of the array while maintaining essentially the same level of null. This imposes additional requirements on the observatory for the required maneuvers to sample the UV plane. These impacts include the complex control loops required to maintain desired accuracy, thermal variations caused by changing sun angles, variations in solar pressure on the sunshields and micro-dynamic effects on both structure and instrument during motion and resettling. Free flying systems also have the impacts of one spacecraft effects on its neighbors. Thermally, the altered position / location of the adjacent spacecraft influence the radiative cooling and generate small thermal drifts in sensitive components. Use of any mass ejection thrust system can apply perturbing pressure or heat on adjacent spacecraft coating surfaces with effluent, pitting shielding and optics or simply altering absorbtivity / emmisivity over time. The shielding requirements end up limiting the sky coverage or driving to very complex and unproven reorientation systems, particularly for the free-flying approach.

1.2.2.1.4   Conclusions

A primary conclusion is that interferometric nulling at the levels needed for the detection mission is extremely challenging. Producing a central null is essentially equivalent to extremely accurate constructive interference. But

TPF requires both a deep central null and a significant width in order to suppress the full extent of the central star. This is performed with a delicate balancing of beams between multiple telescopes. If the challenge of nulling is met, the exo-zodiacal light could still swamp a terrestrial planet's signal since at each orientation the interferometer fringes will include not only planets but also the exo-zodi. Differential schemes such as nodding the interferometer should be investigated if interferometers are selected for further study.

1.2.2.2 Large Aperture IR Coronagraph

A large aperture coronagraph (LAC) is a natural extension of NGST mated to the Eclipse coronagraph technology. The goal is to separate out the planet light from the starlight. This can be accomplished with either a very high resolution system (see the ULSA concept below) or by using a coronagraph to block out a large part of the stellar light (variants are seen in this and the following two sections). For thermal infrared observations, the required diameter of the collecting area can be shown to be 30-40m. For similar observations in visible, a 10m aperture would be sufficient, even with the higher contrast ratio between the planet and star at shorter wavelengths.

In Phase I of the TPF study, we concentrated on the thermal IR coronagraph, but investigated the capabilities of a similar visible system. We performed trades between a fully filled and partially filled aperture, and examined the requirements for wavefront error control, dynamic control, and packaging. We left detailed trades on the exact aperture size and shape for Phase II.

1.2.2.2.1 Concept Description

The primary components of the system are the telescope, the instrument module, the spacecraft, and the sunshade. Key to performance of the system is the dynamic and thermal stability that can be achieved, the aperture size that can be fit into existing launch vehicles, and the size and number of the individual mirror segments.
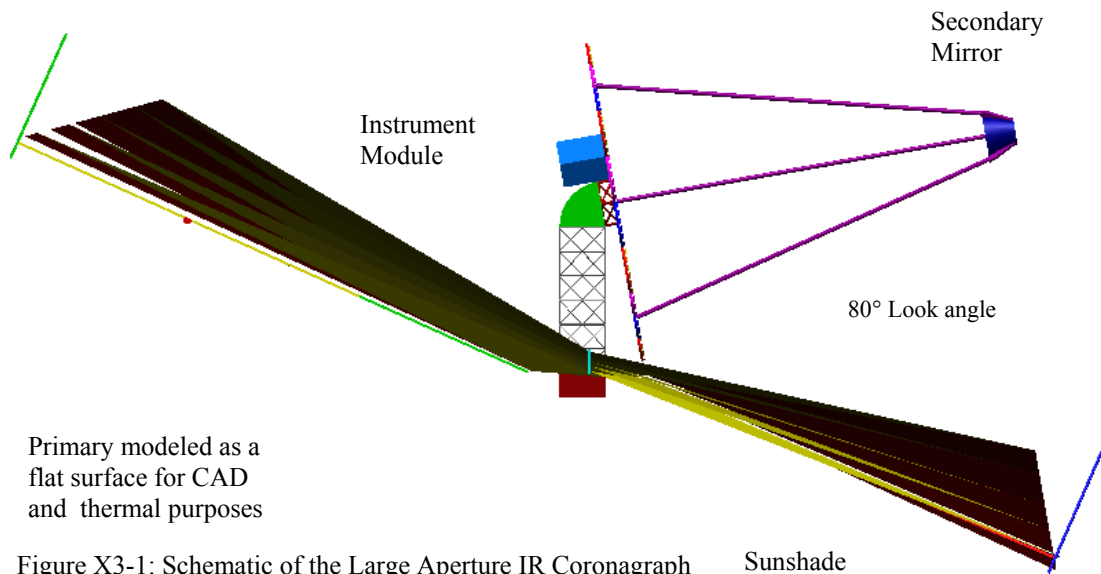

Figure X3-1: Schematic of the Large Aperture IR Coronagraph

The baseline system is a 36 hexagonal section primary with each segment 4 meters flat to flat. We also investigated other sizes of apertures using either larger hexes or an additional ring of hexes. The variations were presented at the PAR. A solution with 18 hexes in the outer ring, each 4 m flat to flat, fits in a single launch vehicle and "existing" (in development) shroud. Mass estimates for the primary mirror used Kodak AMSD technology at 15 kg/m^2. This drove the overall mass of the telescope and was a limiting factor for the total number of hexes that could be launched. The instrument module assumed a coronagraph based on the Eclipse instrument with a spectrometer and allocated additional volume and mass for a guide camera and an additional camera for general astrophysics.

The spacecraft and sunshades were specified based on TRW experience with NGST and other spacecraft designs. Existing subsystems were used to provide proof of concept, demonstrate low risk and to make an estimate of launch

mass and cost, but were not optimized during this phase of the study. These subsystems will continue to improve with time augmenting existing margins but given the timeframe of TPF and the development cycle of new electronics current TPF resources were better spent on the instrument development and technology road map activities. An example, the communications and data handling subsystems throughput are similar to those of NGST and will benefit from work on that program over the next few years.

Based on operational and performance analysis, we believe that an L2 orbit is the best orbit for this system given the Earth relative stability, thermal stability and sky coverage requirements. A 1 AU drift away orbit is also a possibility, but this orbit requires more complexity in the communications system driven by the steadily increasing distance. This impacts sky coverage and has a definite lifetime issue unless the trajectory is stabilized with respect to the Earth distance.

A block diagram for the system is shown in Figure X3-2. We have identified the required control loops for maintaining the image quality and pointing during an observation. The detailed design of these components was left to the Phase II study. However, the driving requirements and the technology development needs have been identified based on the identified components.
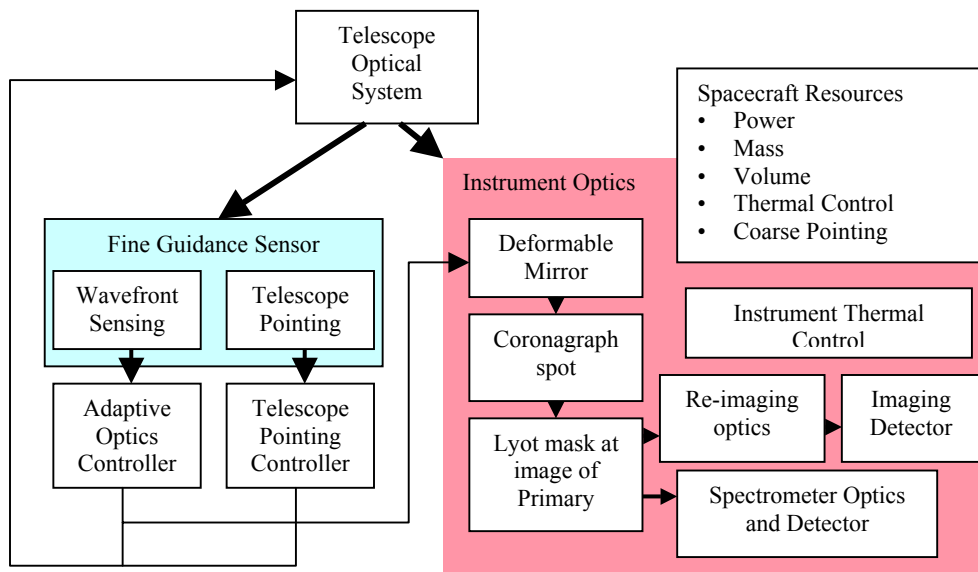

Figure X3-2: System Block Diagram for the LAC.

The operational flow of this system is relatively straight-forward as it is just a telescope. As shown above, the spacecraft is responsible for the initial coarse pointing of the telescope. The Fine Guidance sensor then takes over and does both the job of wavefront sensing and the Telescope pointing. The wavefront sensing and correction is estimated to be a very low bandwidth operation since the changes to it are driven by slow thermal drifts in the primary mirror. At worst we estimate the wavefront sensing correction to have to be applied once per integration time, but more likely once per day or week.

1.2.2.2.2   Performance

We estimated ≤4 hours for the large structure to slew, point, settle, and acquire a target. For this type of architecture, we estimate that we will need more time for the characterization mission than in the detection mission due to the large stellar leakage around the coronagraph spot at the longest wavelengths of interest. Therefore we reduce the average observation time available for the detection mission to 16 hours. With the observation overhead, the total integration time available is 12 hours.

Because the SNR of this system is highly dependent on the angular separation of the planet from the star, the spectral observations will be timed to occur at the most optimal time in the orbit of the planet if at all possible. The architecture also drives the selection of a spectroscopy method that collects the spectra simultaneously, e.g. using a diffraction grating, as opposed to sequentially as with filters. The most likely configuration would be a flip mirror in

the coronagraph optical path that redirects the light to a dispersive spectrometer (as shown in the block diagram). This will be studied more fully in Phase II.

Also taking observing time are the needed calibration observations to ensure peak instrument performance. The L2 orbit provides a large measure of thermal stability and low levels of contaminants so calibration sequences, after the initial system commissioning, should not be required more than once every 2 weeks, and likely only monthly. A calibration sequence would consist of pointing to a known star that is a point source and take image and spectral data using all filters and other variables that are expected to be used between that time and the previous or next calibration sequence. If internal calibrators are used, data with them will also be obtained. The selected star should be very bright to minimize the required observation time. In addition, if other astrophysical observations are to be made between calibration sequences, that instrument should also collect the required series of observations.

We have modeled a variety of configurations and measured the performance against the benchmark of the Solar System at 10pc using a 20% bandpass filter centered at 10 μm. The filter selection can be tuned somewhat based on the spectral type of the star and the anticipated HZ location. We used the available performance models to size the aperture as well as to determine if the concept was within reason for doing the TPF mission as defined in the requirements section. Detailed performance modeling was left for Phase II.

One tool used extensively for sizing the aperture was an IDL routine developed by Dr. C. Bennett on our science team. His model showed that an aperture of 35 m could be used only partially filled (10 m annulus) and still achieve a very high SNR = 44 for Earth at 10 pc in a 12 hour integration time. But with a smaller annulus (5m) the SNR on the Earth was only 3. Since the Earth at 10 pc is among the easier cases for detection in the source sample, a large margin with the current level of fidelity of the model is required to have a reasonable chance of doing the mission. This shows that unless other changes can be made to improve the performance, a single ring of the 36 hex design cannot do the mission, even with a 35 m aperture. At minimum, 2 rings will be required.
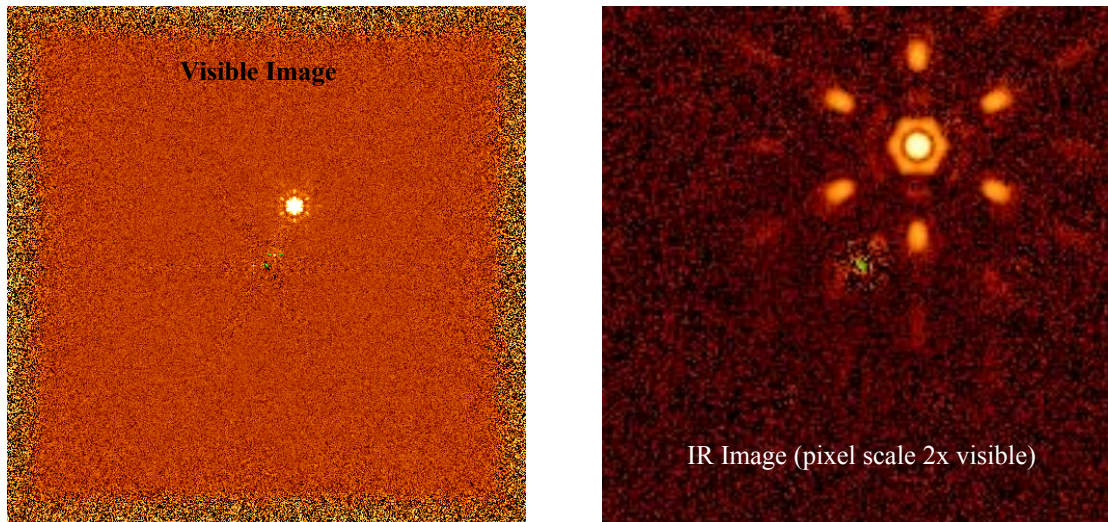

Figure X3-3: IR and Visible images of the Earth at 10pc for the LAC from models developed by Dr. J. Trauger

A more detailed model was developed by John Trauger at JPL based on his Eclipse Testbed model. He modeled a filled 32 m diameter, 36 hex aperture at 10 μm, and a 13.7 m diameter aperture at 0.7 μm case which corresponds to the inner ring of the large IR telescope. His model includes estimates of the WFE of the telescope mirrors as provided by Kodak. He used a gaussian occulting spot with different parameters than C. Bennett's model. This model gives a SNR of 5 on the Earth in ≈ 24 hours of integration time. This model is time consuming so a complete system trade was not performed, but an optimized solution within the tradespace seems very likely. The results for the visible system were roughly equivalent with the IR system, with less contamination of the star in the image.

1.2.2.2.3 Technical Tall Poles

The key technical challenges for this architecture are primarily related to the large optics and wavefront error requirements to do the coronagraphy. Figures X3-4 and X3-5 show the wavefront and figure control required for

both thermal and dynamic errors. Development will be needed in these areas to reach the needed stability for the large structure. This has to be done while minimizing the overall mass of the telescope. The mass of the primary mirror, particularly as the fill factor approaches unity, drives the launch vehicle requirements. Packaging is a major consideration as the largest fairing currently in development is a 5m class, which would limit the mirror hex size to about 4 m flat to flat. Mirror manufacture technology will also have to progress to meet the requirements of this mirror. The large size also leads to difficulty in testing that will have to be addressed.
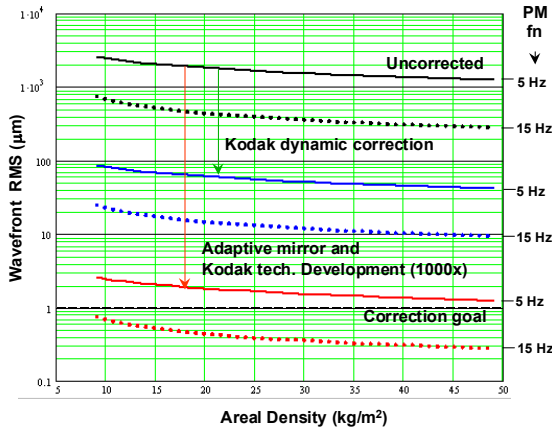
Figure X3-4: Dynamic Correction Requirements
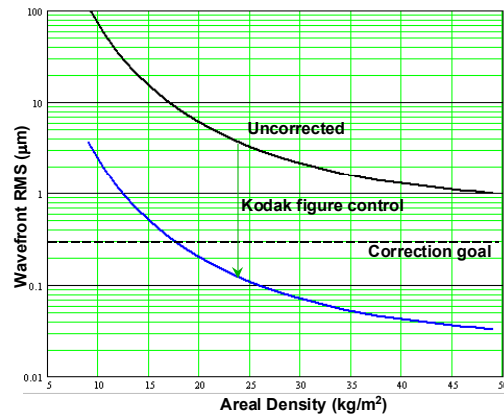
Figure X3-5: Thermal Correction Requirements

1.2.2.3 IR Fresnel Coronagraph

The Fresnel Coronagraph is in essence another realization of the large aperture IR coronagraph described above. The technology and implementation though are sufficiently different for it to be considered a separate concept in the Phase I study.

Figure X4-1: The Fresnel Coronagraph concept with an enlarged view of the Eyepiece satellite
(relative positions not to scale)

1.2.2.3.1 Concept Description

Figure X4-1 shows the basic design of the Fresnel Coronagraph, which consists of a "magnifying glass" collector and a free-flying "Eyepiece" which hosts the instrument package and data handling hardware. Figure X-2 is the

block diagram of the Fresnel Coronagraph, showing how chromatic abberations are corrected in the Eyepiece satellite.

Chromatic aberration of Fresnel Magnifying Glass
is removed with Fresnel Corrector

Figure X4-2: Block diagram of Fresnel Coronagraph

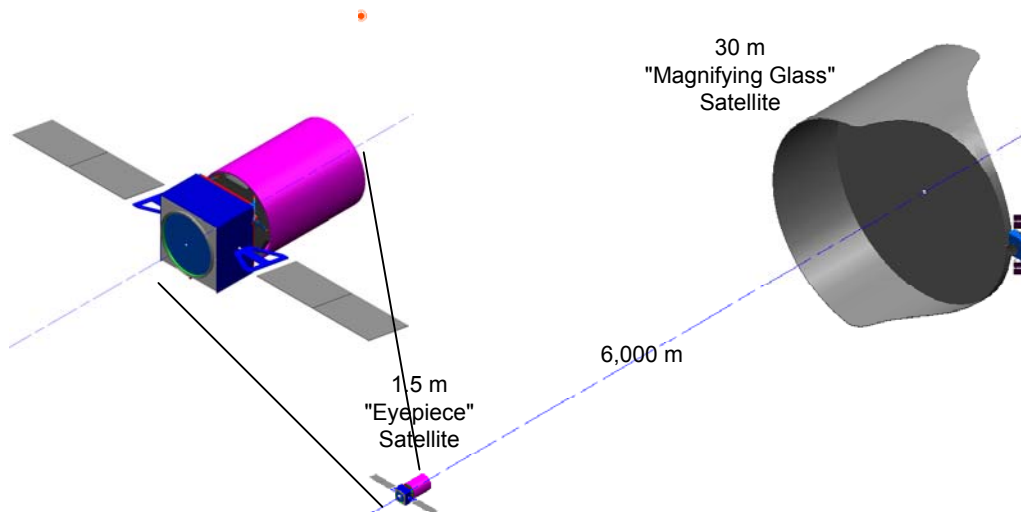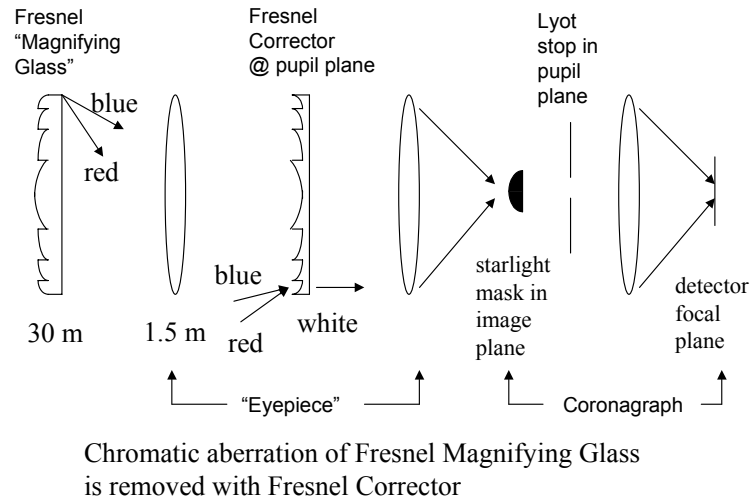The design parameters of the Fresnel coronagraph are as follows:
- Covers spectral range 1-25 microns except 9 ± 0.2 microns and 16.4 ± 0.4 microns
- 30 m aperture
- 104 Fresnel zones
- 6,000 meter focal length (f/200 system)
- 1.5 m secondary aperture
- Fresnel primary and Fresnel corrector are constructed of readily available 0.38 mm thick silicon wafers (commonly available up to 12 inches in diameter)
- Primary may be spun to provide stabilizing tension

1.2.2.3.2   System Operations

The operational scheme for the fresnel coronagraph is very similar to the large IR coronagraph. The main difference is that two elements must be moved simultaneously with the alignment being maintained or re-established after slewing. The alignment tolerances are discussed under performance, but they are quite reasonable and much looser than in the case for the interferometer. The detailed study of how long it takes to repoint and the communication logic between the two satellites was left for Phase II study.

1.2.2.3.3   Performance

The performance of the fresnel coronagraph depends on both the properties of the fresnel optics and the alignment and manufacturing tolerances. Figure X4-3 is the efficiency v. wavelength for the point design system over the 7-17 μm wavelength band of primary interest to TPF. Using Bennett's coronagraph model and the fresnel system for the input with a 0.2 arcsecond (1/e point) gaussian occulting spot, sampling at 0.01" per pixel, a 2 hour integration time, and R = 3 filter at 10 microns, a SNR of 11 is obtained for the Earth. Venus, Mars, and Jupiter are also easily detected. Figure X4-4 is a plot of the flux contributions from the various sources as seen through the coronagraph with Figure X4-5 the image obtained after subtracting the star and zodi contributions.
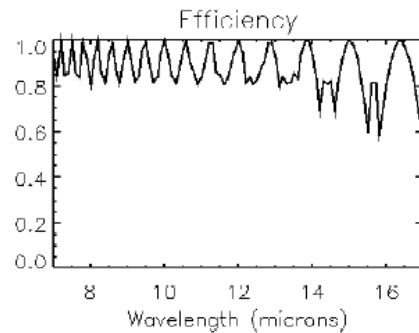

Figure X4-3: The efficiency of the Fresnel Optics is a strong function of wavelength.
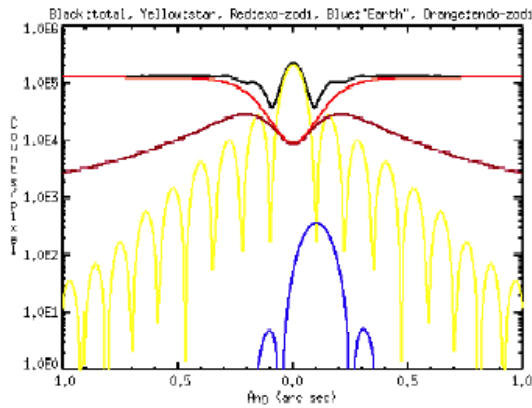
Figure X4-4: All contributors of the scene image are shown individually along with the sum of the signal received through the occulting spot.
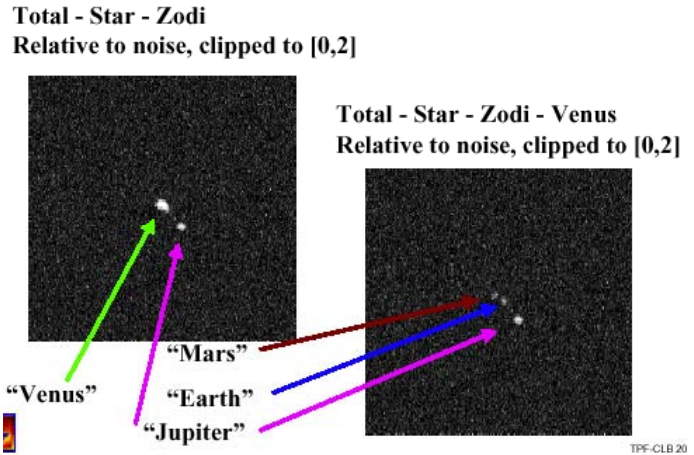

Figure X4-5: Modeled image scenes after star and zodi subtraction showing the locations of each of the detected planets.

The required optical performance to achieve these results was analyzed, as issues arose regarding alignment tolerances, manufacturing tolerances, and scattered light. The calculated error budget for the collector to reach an rms WFE of 1.25 µm at 10 µm are 16 cm of out of plane error, 2 mm of in plane error, and 0.4 µm of thickness variations. While these place stringent limits on the manufacture of the element, the stationkeeping requirements are within those proposed for other systems, with the most critical one, the in plane error, being the easiest to sense and correct for via laser range finding.

Scattered light in the system is almost entirely due to the fresnel corrector in the eyepiece telescope. The estimated degradation of the Strehl ratio due to this scattering is 0.9875 and appears to be within the ability of the system to maintain performance for the targets of interest. Fully implementing this effect into the overall performance model was left for Phase II study.

1.2.2.3.4 Technical Tall Poles

The technical challenges for the fresnel coronagraph are in the areas of formation flying for the two spacecraft and in the manufacture of the large fresnel collector. As noted, the in-plane tolerance between the two fresnel elements is 2 mm. This will be a challenge to maintain while the two spacecraft are 6000 m apart. However, this type of
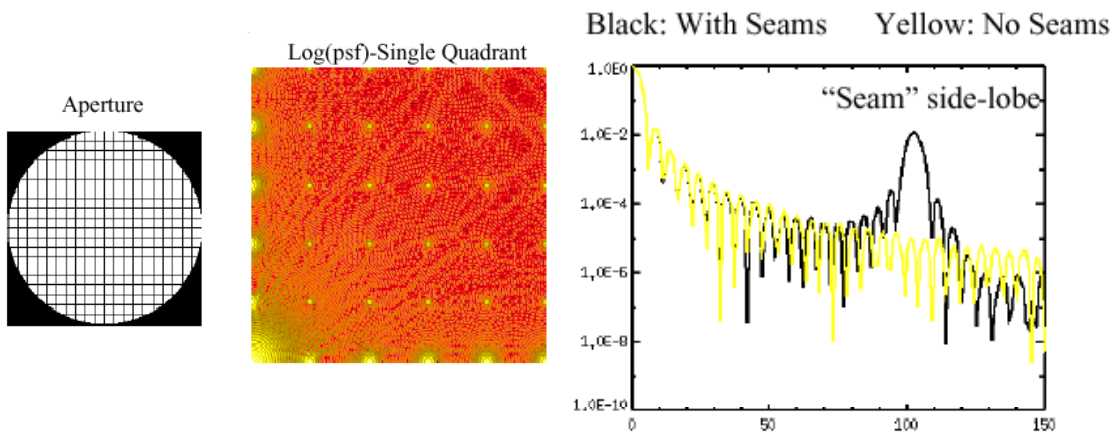

Figure X4-6: Left figure is a conceptual realization of how the Fresnel lens could be manufactured from small, 1m square pieces of silicon. The middle panel shows model output of the resulting diffraction pattern. The right panel shows a cut through the peak of the diffraction pattern of the lens both with and without the seams.

formation flying is being developed under other NASA and the distance between these 2 formation flying vehicles greatly reduce the impingement issues so is not seen as a particularly high risk item. The fresnel development efforts at Lawrence Livermore National Laboratory are currently working the manufacturing issues.

The manufacture of the large aperture is more problematic as currently, the needed silicon wafers are commonly available in only 12 inch diameter pieces. We believe it is reasonable to extrapolate a process to make 1m panels of silicon for the construction of this large lens. These would then be processed to have the fresnel zones and then assembled. The seams for the assembly have been modeled and the effects are show in Figure X4-6. These effects can be accommodated within the data processing algorithms but they do decrease the SNR. The second issue is how to assemble these 1m panels into the full aperture and launch the unit. No simple answer has presented itself during the Phase I study, but construction at the spacestation by astronauts is seen as the most feasible solution. Mechanical deployment of something of this size with the need to have few if any support beams across the aperture did not seem likely.

1.2.2.4 Free Flying Occulter

As has previously been discussed, the difficulty in imaging planets lies chiefly not in the dimness of a planet, but in the brightness and proximity of the associated star. One method of overcoming this contrast that has been suggested is coronography -- bringing the star to a focus and then blocking the stellar light. One difficulty in achieving high contrast imaging with coronography is scattered light due to minor imperfections in the telescope optics. The free flying occulter (FFO) is fundamentally a coronographic concept approach which seeks to avoid the scattered light problem by blocking the stellar light outside the telescope, before it has a chance to enter the optical path.

1.2.2.4.1 Baseline configuration

The general approach for the FFO is to formation fly a large occulting mask in conjunction with a space-based telescope. The occulter is positioned along the line-of-sight between the telescope and a target star. Because of the strong wavelength dependence of diffractive optics, the FFO's nulling performance improves strongly with declining wavelength, so that visible wavelengths are likely the optimum waveband for both detection and characterization. With appropriate design and positioning of the occulter, all but 1 part in 10^9 of the light from a parent star at 0.5 μm is blocked. This allows the direct observation of extra-solar, earth-like planets around solar-type stars out to beyond 10pc. It also permits the characterization of their atmospheres with high resolution spectroscopy, particularly the detection of oxygen, water, and other molecules.
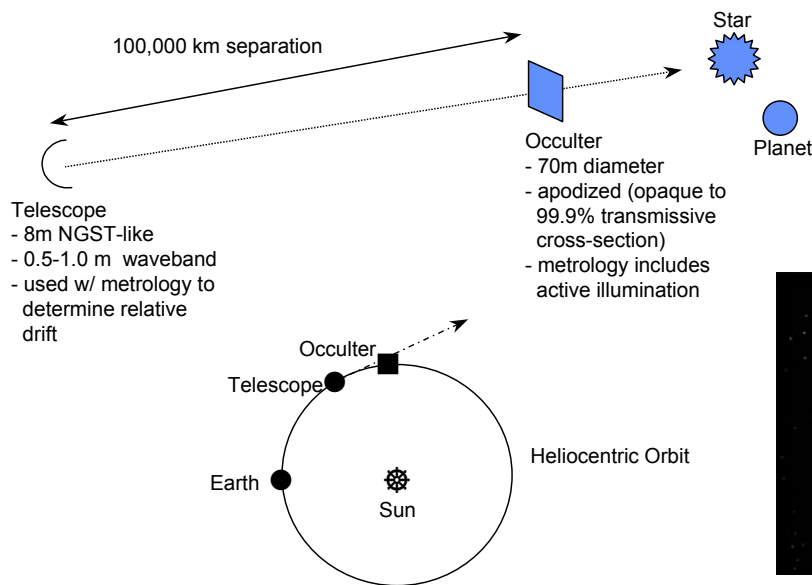

Figure X5-1: The FFO concept using an NGST-class telescope in a 1 AU orbit with a 70m diameter occulter (artist concept shown in inset).

The size of the occulter and the separation between the telescope and occulter is a trade between maximizing the null and avoiding nulling out the planet for close HZ angular separations. Engineering considerations such as cost,

mass, and propellant must also be considered. The solution we studied is a 70x70m occulter at a 50,000-100,000 km separation from the telescope as shown in Figure X5-1. This configuration allows us to detect and characterize Earth-like planets around stars within 25 parsecs of the Sun, probing exo-solar habitable zones of > 70 mas. The occulter design incorporates a circularly symmetric transmission function that is opaque at the center and transparent at the edges. The opaque center houses the spacecraft, and associated systems. The occulting film is square in shape with support struts of 1 to 7 cm in diameter along the two principle axes (inset in Figure X5-1). The perfect occulter has 100% transmission at the edges and 0% transmission at the center. For manufacturing reasons, the maximum transmission was modeled as 99.9% for the baseline case.

For the telescope, we have baselined an 8 m aperture which is diffraction limited over the 0.5 - 1μm waveband. Orbital mechanics suggest either the heliocentric (Earth trailing) orbit shown in Figure X5-1 or an orbit at the L2 point is feasible. The requirements for the telescope include a very high quality optical mirror but minimal thermal control since the system is non-cryogenic. The launch and assembly issues of such a telescope are similar to those for NGST.

1.2.2.4.2   System performance

To evaluate the performance of the FFO, we modeled our solar system at 10 pc and viewed it with the baseline configuration. We assumed the telescope had no internal scattering and 100% efficient detectors. The intensity of the double diffracted starlight (star-occulter-telescope-image plan) and single diffracted reflected planet light (planet-telescope-image plane) was calculated numerically for each pixel in the FOV. The flux in the 0.5-0.7 micron wavelength used for detection was calculated using the blackbody spectrum for the effective temperature of the Sun. The data for the occulted star and the unocculted planets is generated with Poisson noise. We then subtract off the expected image of the occulted star, leaving behind the noise from the occulted star and any planets. Figure X5-2 shows the results for an integration time of 25,000 seconds in a 2x2 arcsec FPV along with the calculated SNR. Saturn (upper right) and Jupiter (center left) are clearly visible. Both the Earth (right) and Venus (above) can be seen near the center of image brighter than the residual noise from the occulted star. Uranus and Neptune are out of the field of view but should sufficient SNR to be observed.

Other techniques can be employed to improve detection capabilities. For example, polarization can be used to separate planetary light from stellar light. Reflected light is partially polarized whereas the light from the star is not. Also, the nulling of the occulter is wavelength dependent. This will modify the occulted stellar spectrum but will not affect the unocculted planetary spectrum.

Planet	S/N
Mercury[a]	N/A
Venus	38
Earth	18
Mars[b]	3
Jupiter	1308
Saturn	722
Uranus[c]	39
Neptune[c]	15

a occulted
b marginally visible
c outside fov--projected S/N

Figure X5-2: 25,000 second exposure with the baseline configuration of the solar system at 10 pc. The FOV is 2 x 2 arcseconds, showing the solar system out to Saturn.

The characterization of a detected planet is accomplished by measuring its spectrum. The original TPF requirements were only for characterization in the 7 – 17 μm thermal infrared wavelength region. Similar molecular lines exist in the visible and we proposed that an R = 50 spectrum would obtain similar information to the thermal IR spectrum. We start with the same solar system as in the imaging case. The reflected solar continuum and expected spectrum of the Earth are modeled per the TPF SWG recommendations. The reflected Earth spectrum plus occulted solar continuum are Poisson sampled and then fit to the unocculted Earth

Figure X5-3: A modeled spectrum as obtained with the baseline configuration of the Earth at 10 pc (100 mas separation) with R=50.

continuum plus the occulted solar continuum. Figure X5-3 shows the R = 50 spectrum with the integration time required for a 5 sigma detection of each line as indicated. Notice that the oxygen feature and a number of water lines can be identified with seven hours or less of integration time,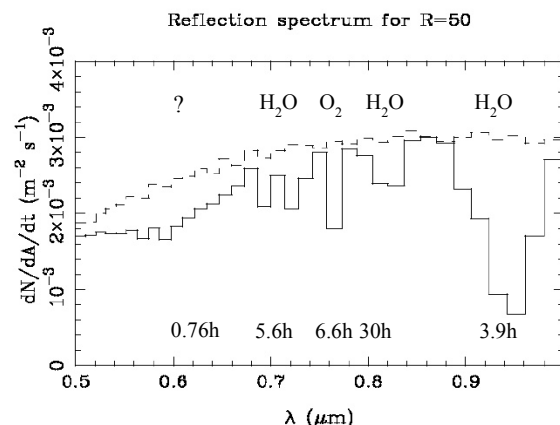 a very reasonable value. Further work by the TPF SWG in Phase II has shown that a slightly spectral higher resolution is required to clearly detect O_2 and CH_4 (up to R = 70). However, this appears to be easily within the capabilities of this architecture given the modeled performance.

1.2.2.4.3 System trades and Technology Development Needs

A configuration with less stringent constraints on the satellite and a 16m diameter telescope for detection and characterization has also been studied. For this system, the maximum transmission at the edges of the occulter was modeled as 99%, significantly degraded from the 99.9% for the 8m case. The results are given in the PAR presentation. In general, we find the apparent contradictory results that an 8m telescope with a very good occulter outperforms a 16m telescope with a poorer occulter. This points to a tradeoff between loosening the constraints on the satellite and increasing the size of the telescope and the integration time. A satellite with tight constraints will perform better but be more difficult and costly it is to build. The detailed trade between these two effects was not performed as part of Phase I and should be addressed to fully evaluate the requirements for an FFO system.

Preliminary studies of orbital parameters shown in Figure X5-4 suggest multiple occulters working independent of each other are desirable to achieve the TPF target and revisit requirements. The highest cost single element of the telescope-occulter configuration is the telescope mirror with cost estimates showing that each occulter will be significantly cheaper than the telescope. The cost delta for multiple occulters is therefore not a great impact to the overall mission cost and allows a much higher observing efficiency of the telescope.
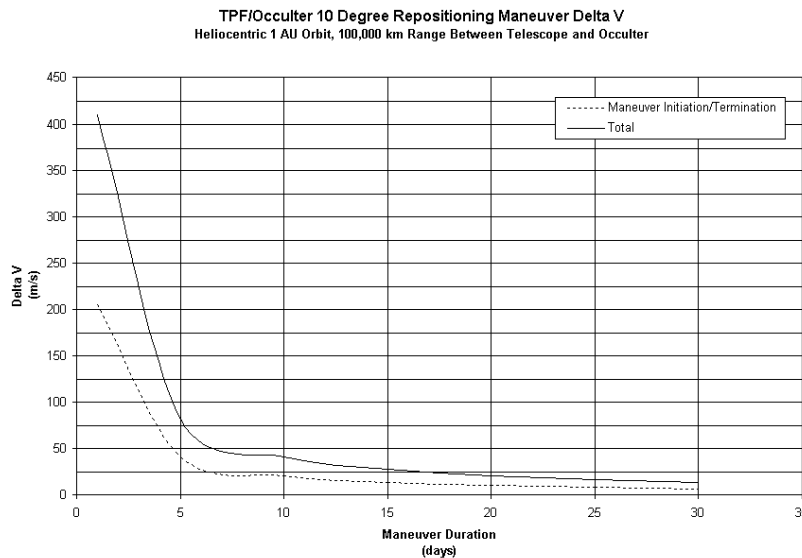
Delta V ∝ f (Observation Duration Period Reposition Maneuver Size)

To minimize Delta V choose
Reposition maneuver duration:
    > 15 days
Observation duration period:
    > 1 month

⇒ > 5 occulters needed
⇒ Delta V ≈ 100 m/s for
    each occulter

Figure X5-4: An analysis of the fuel required to reposition the occulter spacecraft by 10 degrees as a function of the time to maneuver. The time between observations during the detection mission is estimated to be 1 day unless additional astrophysics observations are scheduled.

The two technology needs for the FFO concept are in the area of propulsion / orbital planning and the material selection and fabrication for the occulter itself. These were both evaluated as high risk areas for the FFO.

The first issue is founded in orbital mechanics -- can one (in the L2 or heliocentric earth-trailing or other environment) reposition an occulter so as to occult the line of sight between a telescope and a target star quickly enough and often enough to permit a robust scientific program at reasonable cost in a reasonable time frame. This question has received some attention, and preliminary indications are that even with ion propulsion the answer is yes. . Part of this problem was solved by using at least 5 occulters for one telescope as described above. With the higher ISP's of nuclear propulsion as a possibility recently proposed, the answer is likely to be resounding. As a

related question, can one maintain an occulter aligned for several hours along a line of site within tolerances (≈ 1m) at an occulter-telescope separation of 100,000km. Again preliminary studies suggest a likely approach involving real-time analysis of the occulted stellar image.

The second technology driver is the occulter, both the material required to have the very high transmission at the edges and how the apodization can be accomplished. The occulter demands a variable transmissivity but low scatter film. Achieving that goal may be a challenge. The most promising approach may actually be to distribute holes in an opaque surface. However first basic optics calculations must be performed to determine the necessary hole sizes and distributions. Then material science questions must be investigated. The transmission question is difficult because currently available materials (such as those proposed for solar sails) have a maximum transmission of ≈ 98% uncoated and are susceptable to radiation darkening. The identification of potential materials is an investigation that must be done to verify the feasibility of the FFO concept.

1.2.2.4.4   Conclusions

The FFO allows for a number of precursor missions that can piggyback onto existing missions and fit into existing programs. Possible missions include NGST and SUVO. Performance of an occulter in conjunction with NGST depends strongly on the final NGST configuration as the nulling by the occulter degrades quickly at longer wavelengths and, since the occulter is warm, it becomes the dominant background in the infrared. The PAR presentation discusses this more fully.

In summary, on the scale of TPF architectures, the FFO apparently offers a relatively low risk, low cost architecture for planet detection and imaging in the visible waveband, and with significant ability to conduct a wide range of science. The tall tent poles -- orbital dynamics and occulter manufacture (both materials and apodization) -- have been identified, and are amenable to timely study by readily identifiable experts.

1.2.2.5 Ultra Large Sparse Aperture (ULSA) Telescope

The Ultra Large Sparse Aperture (ULSA) telescope is designed to get very high angular resolution in a single 100 m diameter aperture telescope without requiring the weight and cost of a filled-aperture telescope of similar size. The final design had three spacecraft, illustrated in Figure X6-1: a lightweight monolithic truss structure supporting subaperture elements of the primary mirror, an eyepiece satellite that collected the energy from the primary and contained all the instruments, and a metrology/navigation satellite that would control the positions of the other two and the tilting of the primary-mirror subapertures.

The concept decided upon has approximately 120 4-meter diameter subaperture elements in the primary mirror, which is a fill factor of 19.2%. It was found that approximately 15 to 20% fill factor was required to maintain reasonable control over the PSF artifacts while 100-meter diameter apertures were required for direct imaging of terrestrial planets around nearby stars at 5 to 20 microns. Passive cooling of the mirrors allowed them to operate to about 100 K, which was sufficient for operation over a spectral band from 5 to 20 microns. Since the primary mirror was so large, it was not necessary to operate at fast f/numbers, which would have made alignment a serious issue. The final design operates with an f/5 parabolic primary at wavelengths between 5 and 20 microns. The subapertures elements have spherical figures with active radius of curvature control that allows them to be adjusted to the local curvature of the primary parabolic figure. Parabolic subapertures are not needed. The alignment of the primary-mirror subapertures requires active control only for piston to 25 nm rms, tilts to 4 nrad rms (16 nm rms piston over the subaperture diameter) and
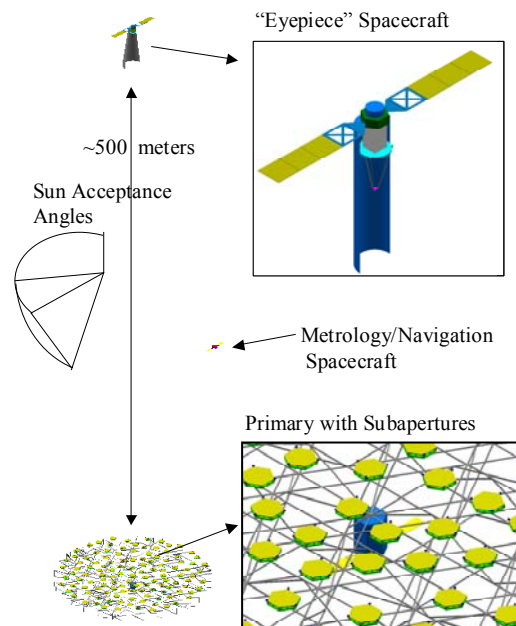
Figure X6-1:   Ultra Large Sparse Aperture Telescope concept

radius of curvature of the primary mirror elements. Three-color metrology is used to control the figure of the primary and the locations of the eyepiece and primary-mirror satellites.

The sparse apertures PSF does have significant artifacts from the sampled aperture, but the magnitude of these artifacts can reduced to reasonable magnitudes if the subapertures are located at "random" positions instead of in a regular array. The PSF resulting from a 19% fill factor with the subapertures "randomly" spread over the aperture subject to a non-overlapping-aperture constraint, is shown in Figure X6-2.
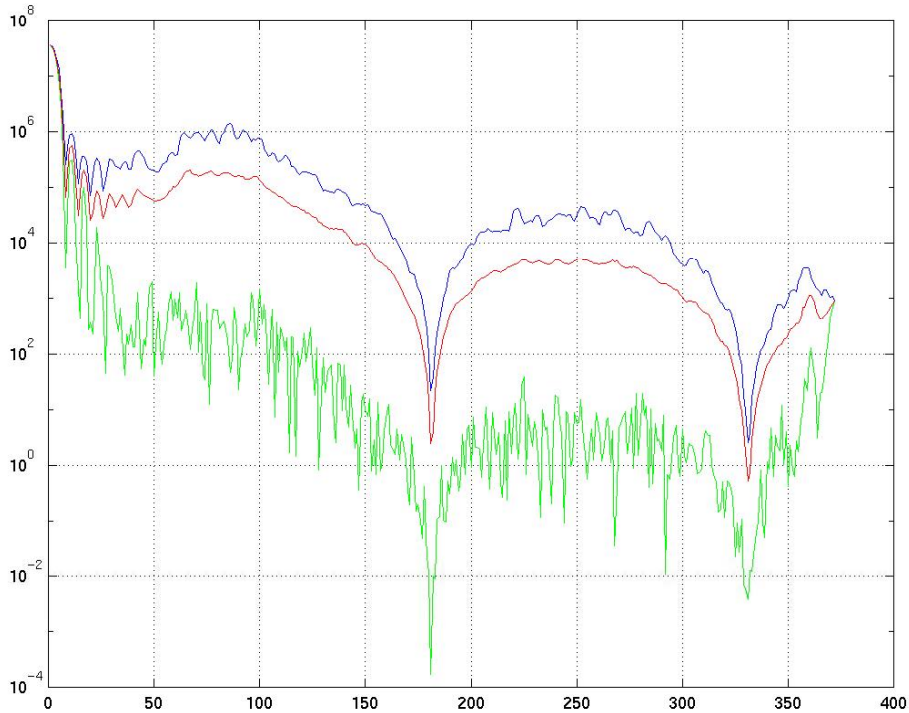
Figure X6-2: Sparse Aperture PSF. Blue curve = max PSF, Green curve = min PSF, Red curve = average PSF. The first Airy ring for the telescope occurs at 179 pixels, which corresponds to 0.0252 arc sec at a 10-micron wavelength.

Planet detection and characterization times were found to be quite reasonable from an operational standpoint assuming the following parameters:
- Sun at 10 pc, Earth at 0.1 arcsec from sun, albedo = 0.38 and Earth's phase is 50%.
- 100-m dia, f/5 primary mirror consisting of 120 4-m dia subapertures randomly distributed.
- 120 K primary-mirror temperature.
- SNR = 5

Given these conditions the detection/characterization times are shown in Figure X6-3.

Figure X6-3: Characterization times for the ULSA as a function of wavelength			
	Time (hours)		
R $(\lambda/\Delta\lambda)$	1.0 μm	8 μm	15 μm
2	1333	-	-
3	2000	2.3	0.4
10	-	7.1	1.2
30	-	21.2	3.6

100	-	70.5	12.1
300	-	211.5	36.2
1000	-	704.9	120.7

The major deficiencies of this system are the close position formation flying of the three spacecraft and the development of the three-color metrology that will have an absolute distance resolution of nanometers over distances of hundreds of meters. The alignment system must be able to do this and also keep the alignment beams directed at the proper subapertures. There is also the issue of producing the roughly 100 large optical elements that have precision control on the order of 1.0 nm rms.

1.2.3 Recommendations

1.2.3.1 Evaluation Results by Metric

After the architectures passed through the "gateway" requirements (can they do the detection and characterization missions, are they technologically feasible for a launch in the 2014-2016 timeframe), they were sized using back-of-the-envelope performance models and a point design was derived. The 6 point designs are described in detail above. Then each architecture was evaluated by the TRW team against the metrics described in section X.1.4. The consensus evaluation is tabulated by metric in Figure X7-1, using the numerical evaluation of High = 3, Medium = 2 and Low = 1. The overall system utility function for each architecture as derived from the evaluation is shown in the bottom row of Figure X7-1, and has a maximum of 90 as calculated (though the maximum is architecture dependent). As shown, the ULSA concept had by far the highest system utility score. The two synthetic aperture concepts had much lower system utility due to system complexity and the effects of confusion in complicated astrophysical scenes.

Figure X7-1: Evaluation of the System Utility Function for the Investigated Architectures						
Investigation	**NIFF**	**NIM**	**LAC**	**FL**	**FFO**	**ULSA**
Science Utility Factor						
Exo-planet detection (4)	1M, 3L	1M, 3L	4 M	4 M	2M, 2H	4H
Exo-planet characterization (2)	1H, 1M	1H, 1M	2 H	2 H	1L, 1M	1M, 1H
Other Astrophysics (3)	2M, 1L	2M, 1L	3 M	3 M	3 M	1H, 2M
Total Science Utility Score	*15*	*15*	*20*	*20*	*19*	*25*
Technology Risk Factor						
Optics Technology (11)	3L, 5M (3 N/A)	3L, 5M (3 N/A)	3L, 3M (5 N/A)	4L, 4M (3 N/A)	3L, 3M (5 N/A)	4L, 3M (4 N/A)
Flight System (9)	2L, 6M, 1H	3L, 4M (2 N/A)	3L, 4M (2 N/A)	3L, 6M	2L, 7M	9 M
Technology Risk Factor Score	*30*	*24*	*20*	*28*	*26*	*28*
Reliability / Redundancy						
# System Elements	11	6	3	6	14	7
Risk Assessment (Low risk elements were not counted)	5H, 6M	5H, 1M	2H, 1M	3H, 3M	2H, 2M	3H, 4M
Rel./Red. Factor Score	*27*	*17*	*8*	*15*	*10*	*23*
Legacy Factor						
Legacy to Life Finder	H	H	H	H	H	H
Legacy to Planet Imager	L	L	M	M	L	H
Legacy Factor Score	*4*	*4*	*5*	*5*	*4*	*6*
Overall System Utility Score	**26.5**	**34.5**	**58.5**	**51**	**49**	**67.5**

1.2.3.2 Ranking

The ranking was done by comparing the overall system utility function to the cost. The cost was developed using NGST and SIM as benchmarks, with complexity scaling factors for each of the major system elements. Figure X7-2 summarizes the basis and complexity factors applied to each system element for the 6 concepts. The overall system utility function v. cost is then plotted in Figure X7-3.

Figure X7-2:   Summary of scaling factors and comparison program by element used to generate cost comparisons for concepts

| Concept	System elements	Quantity	Comparison Program Element	Complexity Factor	Total Cost Estimate (relative to SIM)
NIFF	Collecting Optics	4+	SIM Optics	1 x	4.37
	Combining Instrument	1	SIM Instrument	3 x	
	Collector Spacecraft	4+	SIM Spacecraft Bus	0.9 x	
	Combiner Spacecraft	1	SIM Spacecraft Bus	0.9 x	
NIM	Collecting Optics	4+	SIM Optics	1 x	3.82
	Combining Instrument	1	SIM Instrument	3 x	
	Spacecraft	1	SIM Spacecraft Bus + PSS	1.9 x	
LAC	Telescope	1	NGST Telescope	4 x	2.75
	Instrument	1	NGST Instrument	1 x	
	Spacecraft	1	NGST Spacecraft Bus	1.5 x	
FL	Fresnel Lens	1	Engineering Estimate	1 x	1.38
	Eye Piece Telescope	1	NGST Telescope	0.5 x	
	Instrument	1	NGST Instrument	1 x	
	Collector Spacecraft	1	NGST Spacecraft Bus	0.5 x	
	Eye Piece Spacecraft	1	NGST Spacecraft Bus	0.75 x	
ULSA	Collecting Optics	1	NGST Optics	4x	3.66
	Eye Piece Telescope	1	NGST Telescope	0.4 x	
	Instrument	1	NGST Instrument	1.6 x	
	Collector Spacecraft	1	NGST Spacecraft Bus	2 x	
	Instrument Spacecraft	1	NGST Spacecraft Bus	0.75 x	
FFO	Occulter	5+	Engineering Estimate	1 x	1.95
	Telescope	1	NGST Telescope	2 x	
	Instrument	1	NGST Instrument	0.5 x	
	Occulter Spacecraft	5+	NGST Spacecraft Bus	0.3 x	
	Telescope Spacecraft	1	NGST Spacecraft Bus	1 x	
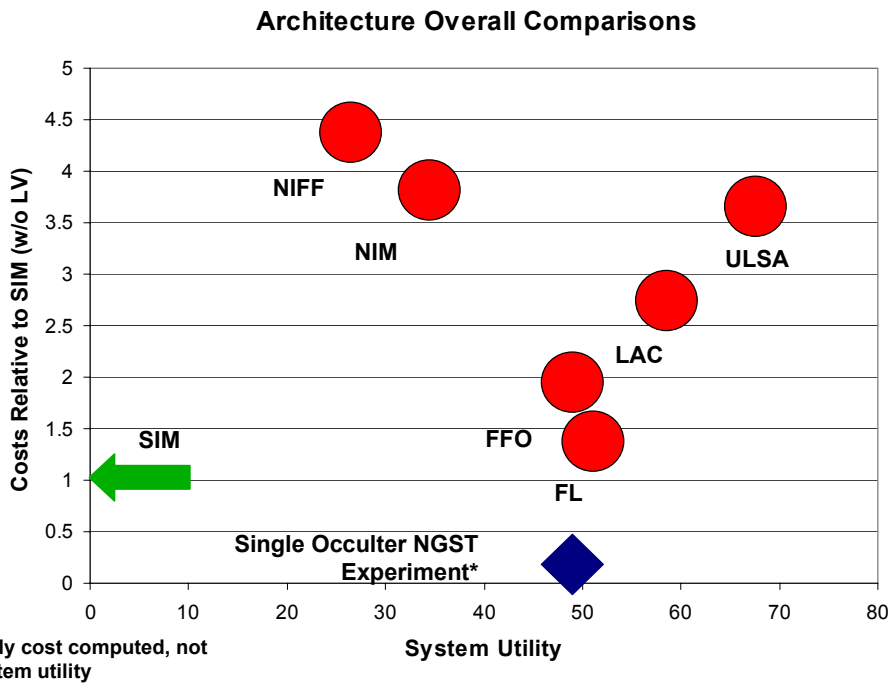
Figure X7-3: The comparison of cost v. system utility for the 6 concepts investigated in Phase I.

1.2.3.3 Selection and rationale

Based on this data, the Fresnel Coronagraph ranks highest based on its low cost and high system utility. Ranked similarly is the Free-flying Occulter and the large aperture coronagraph. Any of these architectures would have been appropriate for further study in Phase II. In retrospect, the FFO may be ranked lower than it should have been given that it received low evaluations for characterization due to the wavelength range. Since the PAR presentations and subsequent work by the TPF Science Working Group showed that the visible is a viable wavelength band to detect the presence of life, the FFO has been re-evaluated with a system utility of 52 compared to 49. This information was not available prior to the PAR so was not included in the concept evaluation process. For comparison purposes, the two coronagraph concepts and the FFO are all equal in science utility to within the margin for error.

The TRW team had some preference for the large aperture coronagraph based on its ability to fully cover the wavelength of interest (3-28 microns, 7-17 microns for the characterization mission) and because of it's heritage to NGST. The ULSA, while quite appealing from a science return point of view, was evaluated to have severe problems with launch, deployment, and cost for the TPF mission, particularly once launch vehicle costs were folded in. The two interferometer concepts were ranked by this method as being very costly with low system utility, primarily due to a low science utility because they are synthetic imagers rather than direct imagers. The confusion due to extended and multiple sources are evaluated as a significant detriment compared to direct imager architectures. The free-flying interferometer concept was evaluated as having a much higher risk with little return for the flexibility in baseline length. A blended concept with mobile collecting apertures on a 100 meter truss was not evaluated but could increase the science utility of the monolithic interferometer with much less increase in risk than for the separated spacecraft version. The Fresnel Coronagraph is an appealing technology, but the team could not devise a method to deploy the primary collecting aperture without use of on-orbit assembly. While it is feasible to employ astronauts to assemble this component, precision assembly has yet to be demonstrated on orbit and, although it is not reflected in the numerical evaluation, this single risk element was seen as a driving requirement. The Free Flying Occulter was also considered worthy of continued study. At the time of the PAR, the orbital mechanics and required fuel to have the occulters efficiently obtain the needed sky coverage was considered a very difficult problem to overcome. Since then, NASA has officially opened up the concept for nuclear powered spacecraft. The use of such a propulsion mechanism for the occulter spacecraft solves many of the issues involved with the occulters. The remaining risk of material selection to obtain the needed transmissivity at the edges of the occulter is still a big unknown. Further study to identify appropriate materials would allow a more realistic evaluation of the associated risks for the FFO.

2   Phase II

2.1   TRW Large Aperture Coronagraph description

During the first phase of our study we examined several different architectures for the TPF mission. These architectures included (1) a > 100-meter baseline IR nulling interferometer with a linear array of four 4-meter cryogenic telescopes; (2) a 30-meter cryogenic telescope with excellent mid-spatial frequency figure and a coronagraph with deformable optics; (3) a 30-meter Fresnel telescope with free flying spacecraft for the primary mirror and modules, separated by ≈ 6 km; (4) a 100-meter sparse aperture IR telescope with ≈ 100 randomly distributed 2 to 4-meter sub-apertures and a separate spacecraft with the correction optics/coronagraph/sensors located ≈ 500 meters away; and (5) a 70-meter apodized occulter flown in formation with an ≈ 8-meter diffraction-limited visible telescope ≈100,000 km away.

From this effort we concluded that (1) the contrast ratio was too severe and the technology development was too challenging for direct detection of Earth-like planets with a visible interferometer; (2) that the contrast ratio in the visible was too severe for the sparse aperture telescope; and (3) that an IR occulter was not practical since the occulter must be very large and very distant from the "camera" telescope.

During the second phase of the study we elected to perform a more detailed study of the IR Coronagraph described herein, while the Ball Aerospace team studied visible coronagraphs, the Lockheed Martin team studied IR nulling interferometers, and the Boeing-SVS studied a "hyper telescope" and an apodized square aperture telescope.

2.1.1   Architecture definition

This section describes the conceptual design for a large aperture telescope with an IR Coronagraph that we developed during the second phase of our mission TPF architecture study. In addition to its capabilities for planet detection, characterization and comparative planetology, this observatory also has a significant capability for general astrophysics in the 3 to 28-μm spectral region.

2.1.1.1 Observatory Configuration

Our conceptual design for a large aperture telescope with an IR Coronagraph is shown in Figure 1. It draws heavily from our previous work for the Next Generation Space Telescope, with a large multi-layer sunshield that allows the segmented deployable telescope and science instrument module to be passively cooled to less than 30K. The primary mirror consists of 36 hexagonal panels measuring ≈ 4-meters flat-to-flat, arranged in 3 rings around a central opening. Each panel has a thin, gold-coated composite membrane mirror mounted attached to a composite backing structure by 6 rigid body actuators for tip-tilt-piston control, and 7 figure control actuators for control of low-order figure errors. The mirrors are produced with a low-cost replica optics process. The panels' areal density is ≈ 5 kg/m^2.
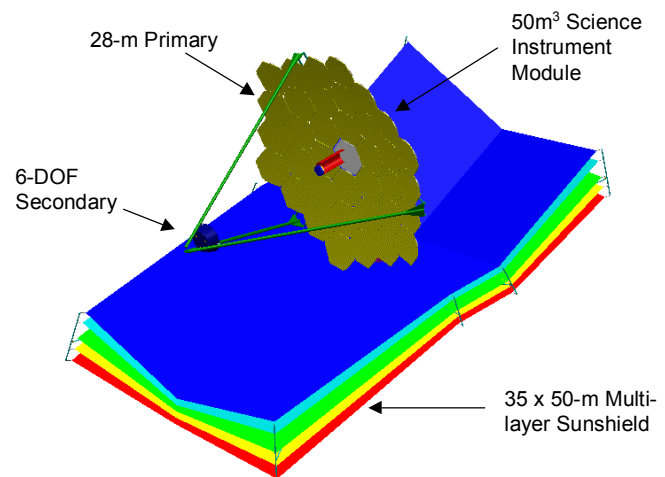

Figure 1. Conceptual Design

A science instrument module (Figure 2) behind the primary houses a coronagraph with an IR imager for planet detection and an IR spectrometer for planet characterization. The coronagraph occupies ≈1/3 of the instrument module's 50 m^3 volume, leaving room for other instruments, such as imagers and spectrometers for general astrophysics observations.
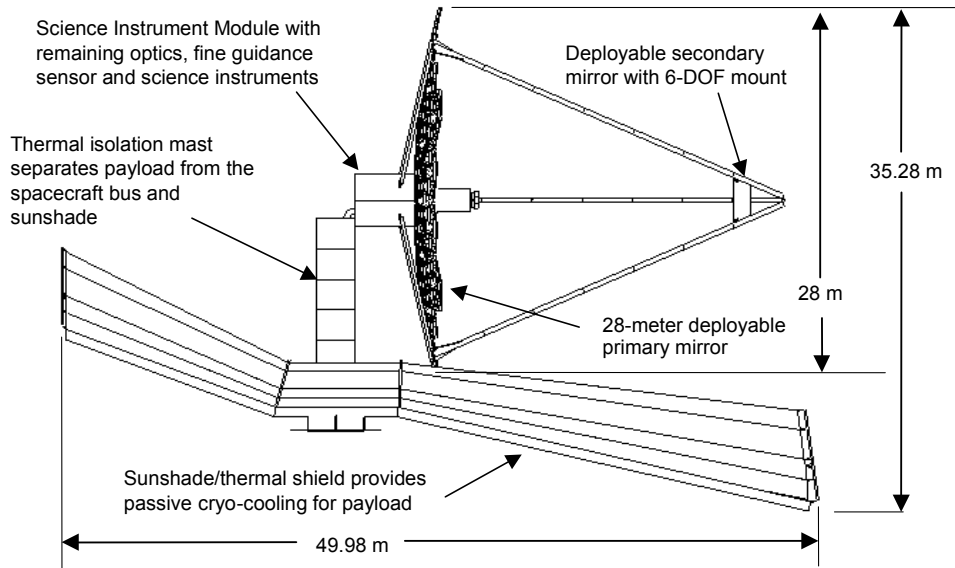
Figure 2. Deployed Observatory (Side View)

This science payload (telescope plus the SIM) is attached to the sunshade and the spacecraft bus by a deployable mast that also provides thermal and vibration isolation from the ≈300K spacecraft with its rapidly rotating gyros and reaction wheels.

2.1.1.1.1 Spacecraft

The Spacecraft equipment compartment (Figure 3) houses all of the avionics and warm payload electronics. A deployable, non-articulating solar array provides constant electrical power while low gain omni antennas
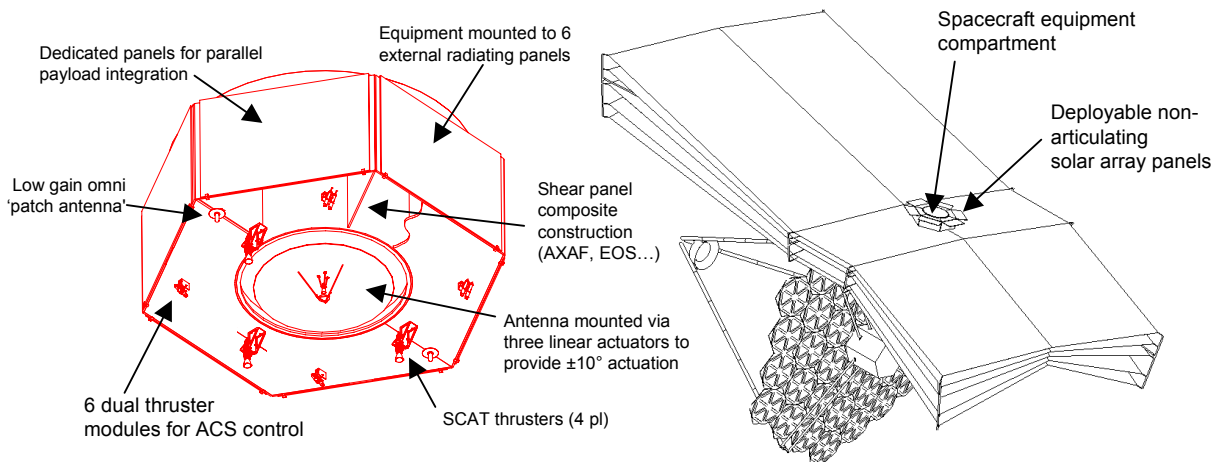
Figure 3. Spacecraft Bus

and a high gain dish antenna provide communications with the ground system. Bi-propellant Secondary Combustion Augmented Thrusters (SCAT) provide propulsion for orbit insertion and station keeping, while hydrazine thrusters provide momentum unloading and backup attitude control. The equipment module has dedicated panels for parallel integration and test. The thermal isolation mast stows in the equipment module's central cylinder.

The entire TPF observatory can be packaged to fit in the fairing of the Delta IV Heavy launch vehicle (Figure 4), which has sufficient lift capability to place it in a transfer orbit to its operational orbit around the L2 point.

replica optics
36 x 0.205 m
7.41 m total

16.5 m

Instrument
4.00 m

sunshade stowage 0.92 m
Spacecraft bus 1.06 m
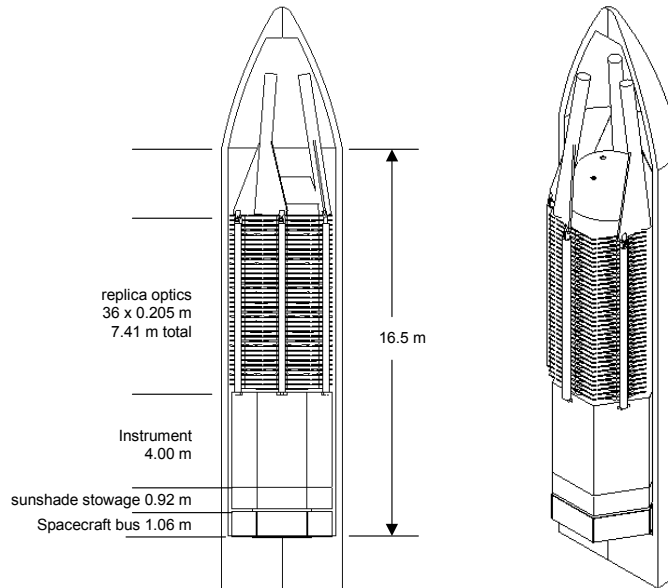
Figure 4. Observatory Stowed in 73.5 foot Delta IV Heavy Fairing

2.1.1.1.2 Deployment

After separation from the launch vehicle's upper stage the spacecraft's solar array panels are deployed, followed by the Optical Telescope Assembly (OTA) and the Thermal Isolation Mast (TIM). The OTA deployment begins with the extension of the telescoping secondary mirror support struts. The struts then hinge in the middle and rotate outward at their point of attachment to the Science Instrument Module (SIM), providing clearance for deployment of the primary mirror. The primary mirror panels are deployed using the approach proven by TRW's highly successful High Accuracy Reflector Demonstration (HARD) Program in the early 1990's. Figure 5 shows how HARD reflector panel stack is raised, rotated, and lowered so that the bottom panel can be latched into place. For TPF this process is repeated until all three rings (36 panels) have been deployed. The secondary support struts are then straightened and latched to the periphery of the primary mirror (see Figure 2). The tertiary mirror, deformable mirror and central baffle

1 **Stowed**

2 **Vertically Separate Stack**

3 **Rotate Stack**

4 **Lower Stack Vertically into Position and Latch to Center Segment**

5 **Repeat Steps** 2 **thru** 4

6 **Fully Deployed**

Figure 5. HARD Reflector Deployment Sequence

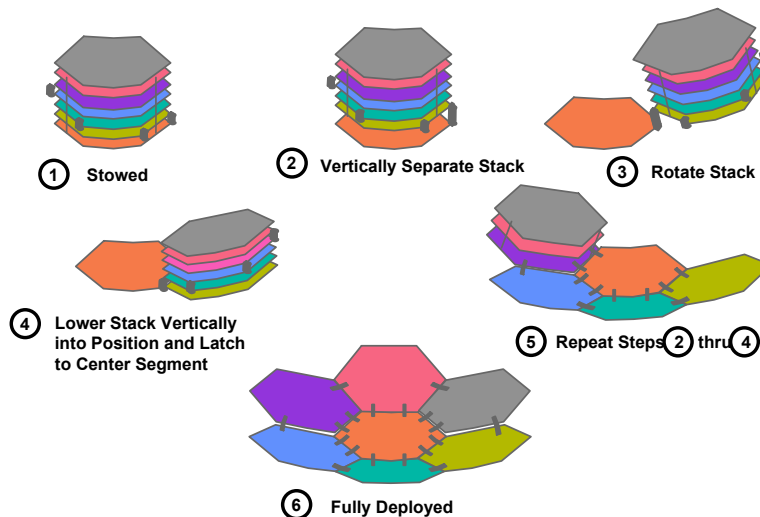that have been stowed in the instrument compartment are then deployed into position with a telescoping mechanism. The final step in the deployment is deployment of the sunshade, using proven mechanical deployment technology developed for large RF antennas.

TPF's 11 deployment systems with 68 elements are not much more complex than those on TRW's Tracking and Data Relay Satellites (TDRS) with 8 systems and 45 elements that deployed perfectly on all 6 flight systems. [In our over 40 years of experience in the design, integration, verification and flight operation of spacecraft deployments we have deployed 672 systems with 1920 elements with a 100% mission success rate].

2.1.1.1.3   Vibration Control

Coronagraphs require a high level of point-spread-function stability in order to maintain the planet-star contrast ratio. Our model calculations indicate we need to achieve ≈ 3 milliarcsecond image stability to detect an Earth at 10 parsecs in 2 hours. This places tight limits on the allowable jitter due to mechanically induced vibrations.

Due to its large size, TPF will have fundamental vibration modes well below 10 Hz. Some modes may interact with the vibration isolator. An active loop in the isolator will enhance suppression of low-mid frequency structural interactions and passive isolation will reject mid-high frequency vibrations. For 6th-7th magnitude stars, sufficient photons reflect from the occulting spot back onto the quad-cell detector to sustain 1000 samples per second, which allows a fine steering mirror loop at 100 Hz bandwidth. Vibratory line of sight perturbations are thus not a major concern.

Defocus and other wave front errors cause the point spread function to leak around the occulting spot, however. The deformable mirror will correct quasi-static wave front errors, but vibratory wave front errors must be suppressed using isolation, stiffening and damping. Figure 6 shows vibration control requirements for the IR Coronagraph versus the system capabilities, and Figure 7 shows our multi-layer vibration control approach.

Design Parameter	Requirement	Capability at Freq. > 10 Hz	Capability at Freq. > 20 Hz
Secondary Mirror Decenter	< 100 nm	14 nm	3 nm
Secondary Mirror Piston	< 30 nm	32 nm	2 nm
Secondary Mirror Tip	< 100 mas	2 mas	1 mas
Secondary Mirror Tilt	< 100 mas	2 mas	1 mas
Primary Mirror Piston	< 2 nm	7 nm	2 nm
Primary Mirror Tip	< 1 mas	1 mas	1 mas
Primary Mirror Tilt	< 1 mas	1 mas	1 mas

Figure 6. Vibration Control Requirements vs. Capabilities
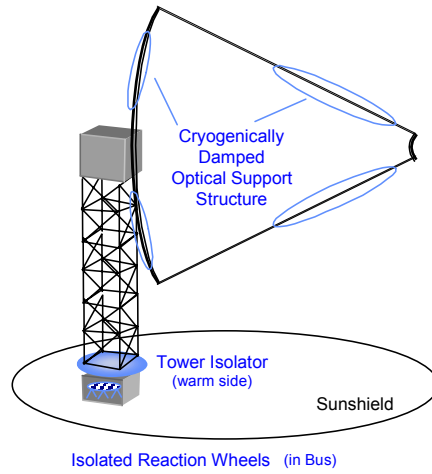
Figure 7. Vibration Control Approach

Multiple layers of passive isolation will isolate vibrations from the reaction wheels at the mounting brackets. The isolation methods are based on technologies developed for Chandra and the Space Interferometry Mission. Active augmentation can provide additional suppression of low-frequency vibrations if needed.

Figures 8 and 9 show some details of our dynamics model, including a detailed structural model of the primary mirror and the overall observatory dynamic model. The results of a typical model calculation are shown in Figure 10.
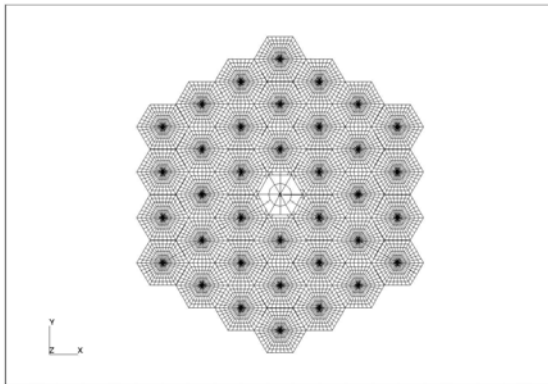
Figure 8. Primary Mirror Structural Model
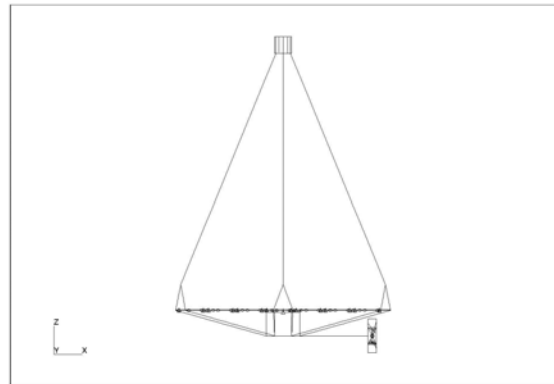
Figure 9. Dynamic Model
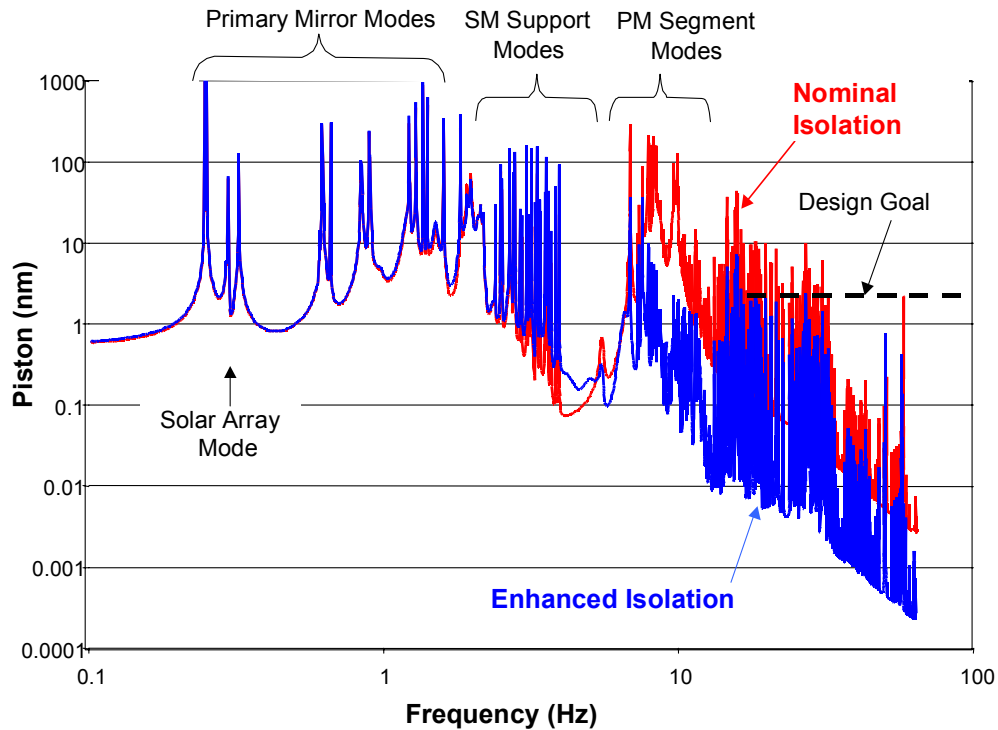
Figure 10 Average Primary Mirror Piston (nm)

With passive isolators the average primary mirror motion is attenuated ≈ 40 dB, and by biasing the reaction wheel speeds we avoid excitation of the primary mirror fundamental and the secondary support structure, solar array and isolator vibration modes. If necessary, additional vibration reductions could be obtained by adding tuned mass dampers, or using adaptive feed forward vibration control.

2.1.1.1.4 Thermal Control

Our IR Coronagraph utilizes the passive cooling approach we developed for the NGST program. By locating the observatory in a halo orbit at L2 we avoid thermal inputs from the Earth and Moon, and we minimize solar heating with the multi-layer sunshade shown in Figure 2. Figure 11 shows the basic thermal requirements for the IR Coronagraph, along with the capabilities of our design. TRW's passive TPF thermal design satisfies all key thermal requirements and builds upon IR&D thermal vacuum testing of our sunshield design approach. The temperatures of the primary mirror elements (Figure 12) range from ≈ 10K to 40K, depending on their view to cold space and proximity to the spacecraft and ≈ 60K sunshade. These temperatures show little variation as the spacecraft attitude changes, however, with an average hot-to-cold ΔT for the PM elements of 0.23K, and a maximum ΔT of 0.31K.

Design Parameter	Requirement	Capability
Maximum Temperature of Primary Mirror Elements	< 70 K	21 K average 40 K maximum
Maximum Hot-to-Cold ΔT of Primary Mirror Elements	< 1.0 K	0.23 K average 0.31 K maximum
Maximum Temperature of Secondary Mirror	< 70 K	25 K
Maximum Hot-to-Cold ΔT of Secondary Mirror Support Struts	< 1.0 K	0.11 K minimum 0.15 K maximum
ISIM Temperature	< 30 K	Can reject 0.62 W with radiator @ 30 K

Figure 11. Thermal Design Requirements vs. Capabilities
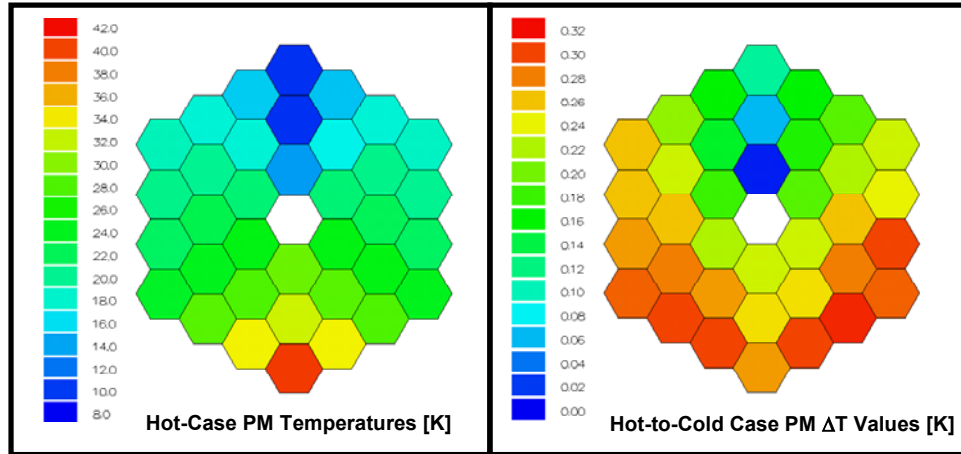
Figure 12. Bulk Temperature and Thermal Stability of TPF Primary Mirror Elements

It is worth noting that the thermal time constant of the primary mirror and its supporting backplane is approximately 100 hours. This is illustrated in Figure 13, where the dimensionless temperature on the ordinate $[(T_{current} - T_{final})/ (T_{initial} - T_{final})]$ requires ≈ 240 hours to drop to zero (i.e.: stabilize). During a typical attitude change and the following viewing period, the expected change in PM temperature is 0.05K or less. The low inherent CTE of the PM elements and backplane structure, combined with a very low ΔT during observatory attitude changes, results in a very optically stable telescope.
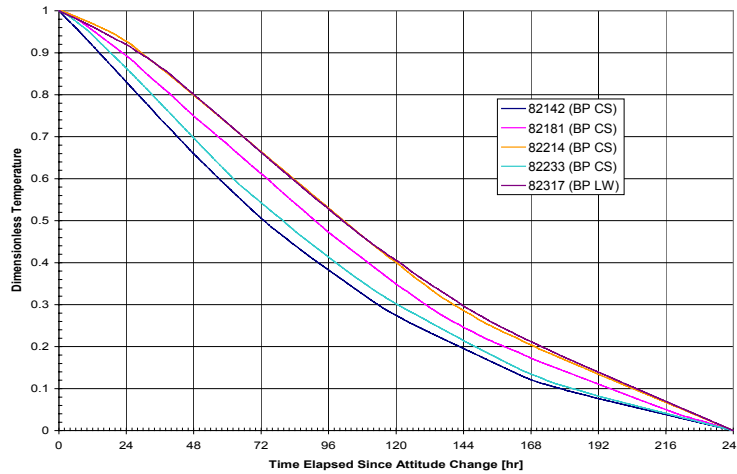
Figure 13. Predicted Temperature History for PM Backplane After an Observatory Attitude Change

2.1.1.2 Telescope description

The Optical Telescope Assembly (OTA) shown in Figure 14 is a three-mirror anastigmat (TMA) with a fourth (steerable and deformable) mirror that provides fine pointing and wavefront error correction. The off-axis in field, on-axis in aperture design provides excellent stray light control and well corrected aberrations in the focal plane with residual spot sizes < 0.038 x diffraction limit at 7 µm over a 2.4 x 7.2 arcminute field of view. The F/20 optical system provides a plate scale of 0.367 arcsec/mm at the telescope focal plane.

The OTA image quality requirement is diffraction limited at 7 µm (with a goal of 3 µm). In order to minimize scattered light the surface roughness requirement is < 10-nm rms (with a goal of 3 nm). The IR coronagraph requires correction of spatial frequencies from ≈0.8 to 98 cycles/diameter. Our actuator

density study show 7 figure actuators are ample for correcting low order deformations such as RoC, astigmatism and trefoil, and we can use global influence functions to control low-spatial frequencies from 0.5 to 10 cycles/dia. The residual is corrected by the DM with ≈200 actuators/dia. The TMA system wavefront error due to actuator residual errors, static wavefront errors, launch induced errors and on-orbit thermal/structural errors (with contingency) is ≈980 nm rms (0.14λ at 7 μm). After correction with the DM the mid-spatial frequency wavefront error is predicted to be 3.69 nm rms. Our Top-Level error budget is shown in Figure 15.

Figure 14. Optical Telescope Assembly Layout

Figure 15. Top-Level Wave Front Error Budget

2.1.1.3 Instruments

The options for the TPF instrument complement are quite diverse. Figure 16 shows a selection of potential instruments one could consider for a large aperture coronagraph. The instrument complement is assumed to
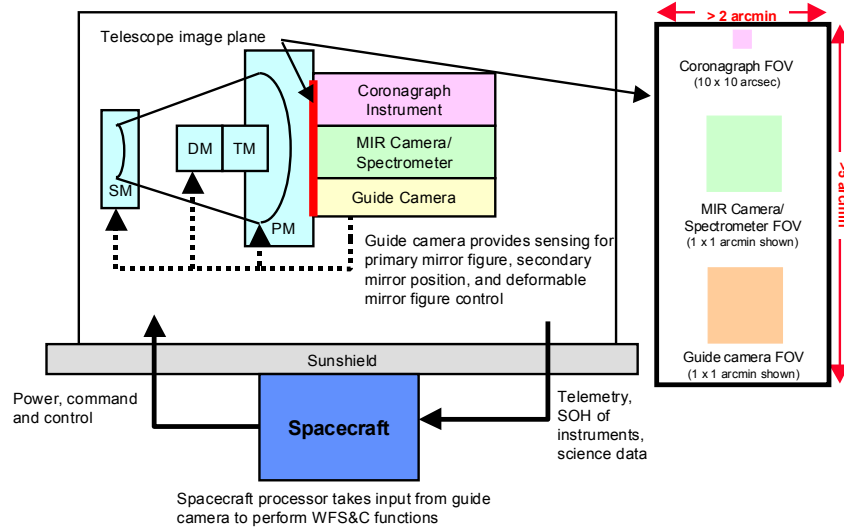
Figure 16. Functional Block Diagram
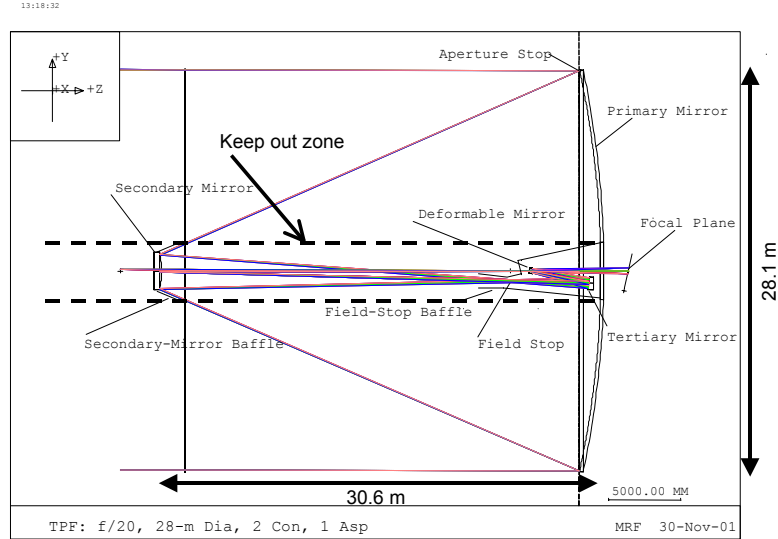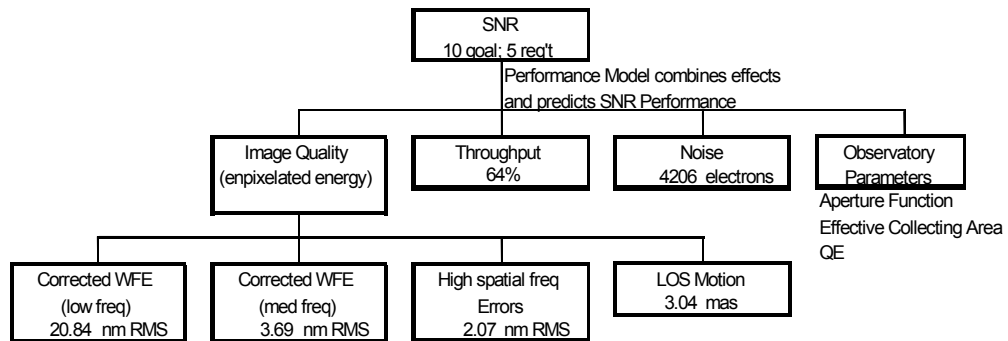
include a guide camera (2 modes), Coronagraph imager / spectrometer, and a wider-field general astrophysics imaging camera. Other possible instruments are discussed in Section 2.3.1.3.5. Figure 17 lists the science instrument characteristics, including the coronagraph, guide star sensor and the optional mid-IR camera/spectrometer. Included in the table but not selected for the strawman instrument complement is a NIR camera. The implementation of such a camera is strongly dependent on the image quality delivered at those wavelengths by the primary telescope optics (currently estimated to be diffraction limited at 7 μm, with a 3 μm goal).

	λ (μm)	IFOV (mas)	FPA size (pixels^2)	FOV (arcsec^2)	Comments
Guide camera (wide and narrow field modes)	3 – 5	60 (w) 10 (n)	1024	60 (w) 10 (n)	HgCdTe or InSb possible detector materials. Readout must run fast enough to drive the mirror for guiding.
IR Coronagraph	7 – 17 5-28 goal	20	512	10	Base on Eclipse testbed heritage. Filter wheel and occulting spot wheel to optimize detection. Dispersive grating spectrometer or integral field unit are options.
IR Imaging Camera / Spectrometer	5-28	60 or 30	1024 or 2048	60 or 120	Use largest available Si:As detector. Options available to maximize instrument flexibility without unnecessary complexity.
Vis/NIR Imager (not included in baseline)	0.5-5	15	4096 (NGST based)	60	InSb or HgCdTe detector developed for use on NGST. Waveband driven by deliverable image quality by primary mirror.

Figure 17. Science Instrument Characteristics

2.1.1.3.1   Guide Camera

A Guide Camera in the focal plane of the telescope is necessary to acquire the target, to provide coarse alignment of the target in the coronagraph, and then to provide coarse guiding for the duration of an observation. The guide camera provides input to the feedback loop to the tip/tilt of the secondary mirror, and the steerable function of the deformable mirror, if it is included.

The guide camera operates in two modes: wide field for acquisition and coarse guiding and narrow field for fine guiding. The fine guide mode is used during observations with instruments that do not have their own fine guiding capability. The coronagraph in our baseline design (section 2.3.1.4.2) includes a fine guidance sensor and pointing mirror. If the coronagraph is the only TPF instrument, the guide camera will only have the wide field mode.

We plan to guide in the $3 - 5$ μm wavelength band to minimize impact on the rest of the system. This assumes the telescope will deliver reasonable image quality at these wavelengths even if it is diffraction limited at 7 μm. Using a longer wavelength band for guiding is certainly possible, but the smaller PSF at the shorter wavelengths will permit more accuracy for the fine guidance mode. Both InSb and HgCdTe detector can be used for the $3 - 5$ μm wavelength band, and 1024 x 1024 pixel devices are currently commercially available in either material. The guide camera detector must be able to read out a small area ($\approx$ 10 x 10 pixels) at a fast enough rate to provide updates to the line of sight pointing mirrors, particularly for the fine guiding mode.

A simple camera system is sufficient for the wide field acquisition mode. Our analysis of star density and limiting magnitudes with reasonable readout rates (100 Hz for the fine guiding mode) indicates a 1 x 1 arcsecond field of view is sufficient over most of the celestial sphere. A larger field of view would be desirable, however; if larger detector formats are available without stressing the data processing algorithms, and it would provide additional margin. This trade should be done when the technology development programs are more mature and pathfinder programs such as NGST are much further along in their design and manufacture.

Two mechanisms must be added for the fine guiding mode: a field lens or a second set of imaging optics to provide the magnification between the two modes; and a steering mirror to allow the fine guiding mode to image any part of the larger acquisition field of view. Design alternatives such as higher pixel resolution versus a larger format device can be traded during the Phase A study.

2.1.1.3.2   Coronagraphic Imager and Spectrometer

The heart of TPF is the coronagraphic imager and spectrometer that will obtain the data for terrestrial planet detection and characterization. Our concept for the coronagraphic imager is based on the Eclipse testbed, with optimizations done to accommodate our 28-m telescope, and provide the desired field of view and pixel size. Figure 18 shows the optical layout for the imaging portion of our coronagraph, including the positions of several mechanisms: a filter wheel; a wheel with several Lyot masks; a wheel with a selection of occulting spots; and a fine steering mirror. There will also be a flip mirror (not shown here, see Figure 19 below) near the chromatic corrector plate, to steer the beam into the spectrographic portion of the instrument. The fine steering mirror is controlled at $\approx$ 20 Hz bandwidth by the reflection of the star off of the back of the occulting spot. The reflected light is focused on a quad cell and a simple maximization algorithm is applied to keep the star image centered on the occulting spot.
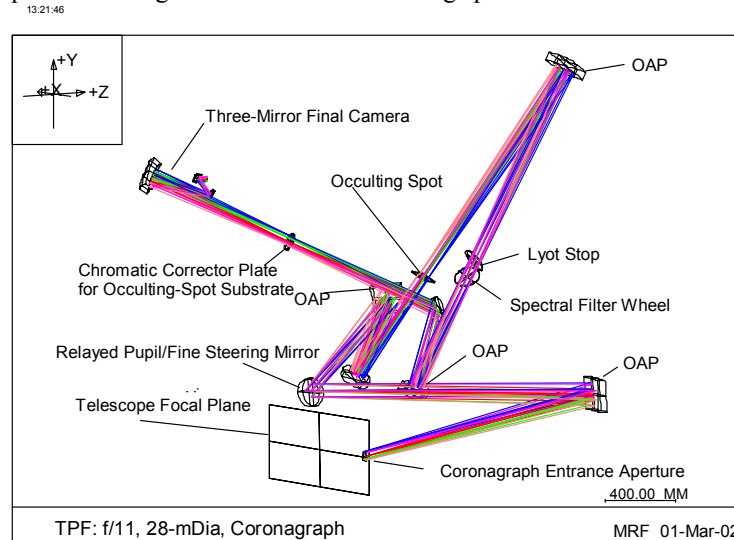

Figure 18. Coronagraphic Imager Layout

Having several filter and occulting spot options allows us to optimize system performance based on the expected location of terrestrial planets, distance to the star system, and spectral type of the star. Larger occulting spots may also be included for use with other targets (e.g. T Tauri stars) where the environment is of interest but the bright central object is slightly extended. An optimized Lyot mask will be available for each occulting spot, to minimize passing diffracted light from the telescope and occulting geometry.

The detector of choice for the coronagraphic imager is a Si:As BIB detector that can cover the entire 3 – 28 µm spectral band for general astrophysics observations, and provide good performance over the 7 – 17 µm waveband. These detectors operate at 10 K, and require the new generation of active coolers that are being developed for several future programs. Current Si:As detectors have 256 x 256 pixel arrays, so a 512 x 512 device should be available for TPF with a modest technology development program. Matching the airy pattern to the detector with Nyquist sampling at 7 yields a plate scale of 25 mas per pixel. This provides a planet-star separation of at least two pixels for a 50-65 mas Habitable Zone (HZ). We selected a detector pixel pitch of 30 µm, which is within current capabilities.

This detector selection is subject to trades when the detection parameters are fully parameterized. It would be advantageous to use a HgCdTe detector with a 12 – 14 µm cutoff instead of a Si:As BIB detector because the quantum efficiency of HgCdTe detectors and their operating temperature are much higher (≈30 K), avoiding the need for additional detector cooling. This selection would limit the spectral band pass for detection (and any other observations made with the coronagraphic imager), however, to approximately 7 – 12 or 14 µm. The science community's acceptance of this limitation in exchange for a reduction in complexity and increased performance in the 7-14 µm region has not been explored.

The spectrograph shown in Figure 19 is a simple dispersive system that employs a multi-object slit mask located at the intermediate focal plane. This device is based on technology being developed for the NGST Multi-Object Spectrometer. We baselined a microshutter device, but intend to incorporate whatever technology is validated by the NGST program.

The dispersive element is tentatively identified as a grating, but it could also be a prism. The advantage of using a grating is that it can be used in the 2nd order for the 6 – 12 µm band and in 1st order for 12 – 24 µm with a dispersion ½ that of the shorter band (0.4 µm / pixel). The present design, however, uses a grating with 2.291 lines/mm and 30-µm pixels giving a spectral resolution of 0.1 µm / pixel from 6 to 12 µm to cover the needed spectral band for minimal characterization (c.f. section 2.3.2.5), and a spatial resolution of 36.9 milliarcsec / pixel. This was the best fit to the desired values of 25 milliarcsec / pixel and 0.2 or 0.4 µm / pixel using a design that only incorporates the natural anamorphic magnification from it's off-axis design. The limiting resolution of the grating, however, is about 42, so the pixels must be aggregated in pairs to get the maximum useful resolution of 0.2 µm. However, by replacing the final imager in the spectrometer with a three-mirror anamorphic design, we should be able to design a system that at least reaches a spatial resolution of 25 milliarcsec / pixel and a spectral resolution of 0.2 µm / pixel. The present design covers a square FOV of 14.4 arcseconds.

Promising targets can be initially characterized in the 6 – 12 µm band, then further characterized in the 12 – 24 µm band if desired. The spectrograph will use a second 512 x 512 Si:As BIB detector, identical to the one in the imager. The required spectral coverage and available slit masks will limit the field of view of the characterization instrument, but not significantly (a radius of 4 arcseconds vs. 6 as in the imager).
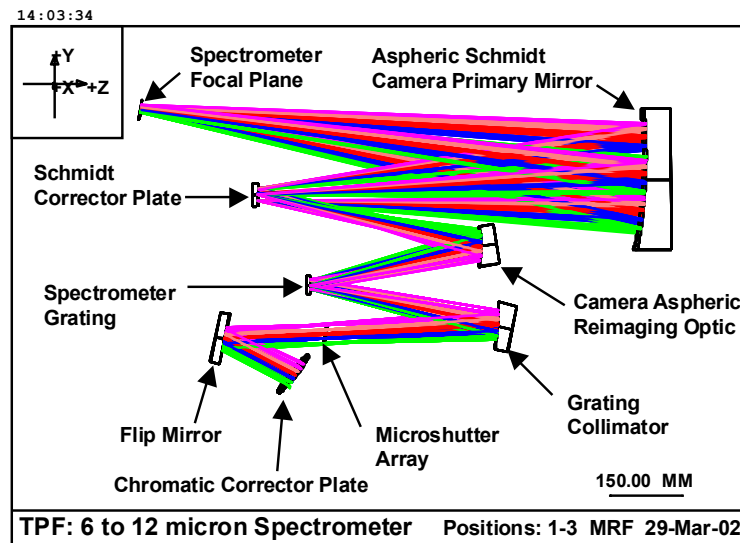
Figure 19. Spectrometer Layout

2.1.1.3.3   General Astrophysics Camera

A wide field imaging camera with a spatial resolution that samples the image at ≈ 2 pixels per airy disk would significantly increase the general astrophysics utility of our Large Aperture IR Coronagraph (LAIRC). It would have a much larger field of view than in the coronagraph and be more sensitive to fainter and / or extended targets. A wide range of filters could be provided to enable a broad range of scientific investigations. We propose using the largest Si:As BIB detector available at the time of the instrument design. A 1024^2 device with 60 mas per pixel resolution would provide a 1 x 1 arcminute field of view. This camera would rely on the fine guiding mode of the Guide Camera to maintain line of sight errors to < 7 mas (1 sigma diameter) which maintains good image quality at the design resolution. This camera is not necessary to perform the TPF mission, but would provide excellent additional science capability if the necessary resources were available

2.1.1.3.4   Other Instrument Options

There are many option beyond our baseline instrument suite for the LAIRC that need to be traded against the desires of the science community and a more complete set of requirements (when developed) with respect to mass, volume, power, and performance. However, a few of our Phase II trades regarding the implementation of the spectroscopy method used by the coronagraph are worth discussing here.

A simple option is to modify the baseline design to move the flip mirror that directs the light into the spectrometer from its current location into a position in the filter wheel. This would eliminate one mechanism from the optical path. However, it would add size to the filter wheel to accommodate the needed angle of the mirror (rather than near normal as for the filters) and would add volume, mass, and cost associated with an additional set of imaging optics. As there are only 2 mirrors that would be added, the savings associated with the mechanism may be an attractive trade, particularly since there are also electronics and heat dissipation associated with any mechanisms that are unwanted in the cryogenic environment.

Another option is to put in symmetrical spectrometers that would allow simultaneous coverage of the 6-12 and 12-24 μm wavelength bands. This would have to be traded against the significant increase in cost, volume, and mass associated with having two detectors and two complete optical trains after the slit mask, but it would reduce the complexity since each spectrometer would have no moving parts and the relative

alignment should be very good. Also, splitting the band would allow the 6-12 μm band to use a HgCdTe detector that has a much higher quantum efficiency than the Si:As BIB device, and does not require additional cooling. Performance modeling indicates that the detector advantage could make the trade worthwhile if spacecraft resources are available.

Finally, an integral field unit (IFU) that would provide imaging and spectroscopy simultaneously could replace the three-mirror final camera and the spectrometer in the coronagraph. Dr. James Larkin at UCLA developed this option (Figure 20) for our LAIRC. His strawman concept covers a 3.5 x 3.5 arcsecond field of view of 118 x 118 spatial locations with 30 spectral channels at each location over the 7 – 17 μm
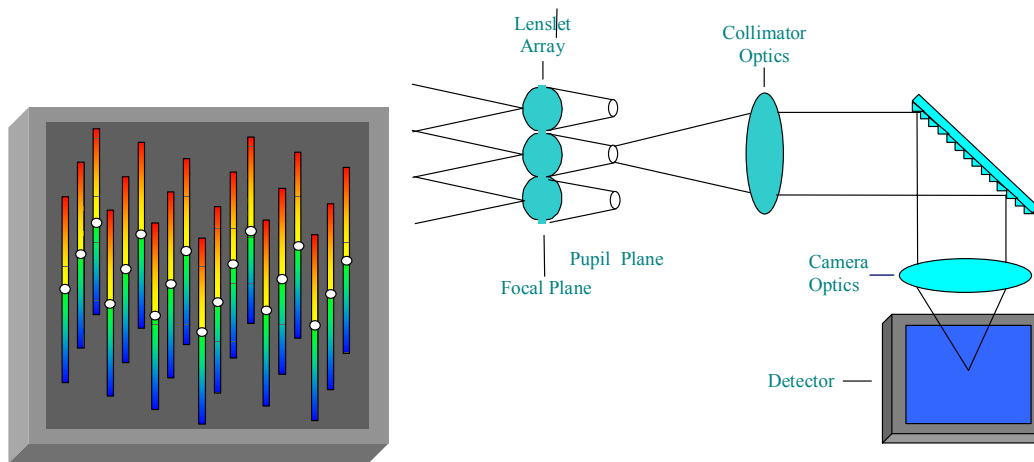
Figure 20: A conceptual layout of an IFU for the LAIRC

waveband for a plate scale of 30 mas/sample. The design has a 1024 x 1024 Si:As detector to ensure that the spectra are not overlapping. A broadband image is easily extracted from the data by summing the relevant spectral bands for each spatial location. The advantages to such a system are that there are no moving parts to obtain both the image and the spectra. Disadvantages include a potentially lower transmission through the system due to more transmissive elements, the larger focal plane needed to ensure the spectra do not overlap, and the smaller field of view obtained. However, the enhanced ability to reject artifacts and to subtract the starlight using spectral features and lack of moving parts may overcome these shortcomings. Further performance modeling is required to determine the mission impacts of using an instrument such as this one.

2.1.1.4 Launch and Commissioning

Our mission concept for the IR Coronagraph requires us to place the ≈ 10,000 kg observatory into an L2 Halo orbit. We evaluated two launch options: a single launch with an Evolved Expendable Launch Vehicle (EELV) into a L2 transfer orbit; and separate launches of the observatory and the upper stage with EELV's and/or the Space Shuttle followed by final assembly on-orbit in a Shuttle parking orbit or at the Space Station. The considerations that went into this trade included: potential benefits of astronaut assistance in LEO, whether deployment occurs before or after major Δv maneuvers; avoiding of excess g forces at burn out of injection stage; and when and where to deploy and checkout the observatory, including verification of wavefront sensing and control systems and science instrument performance.

Our selected approach is illustrated in Figure 21. After launch into an L2 transfer orbit, we separate from the upper stage, deploy arrays and point the spacecraft toward the sun. Following spacecraft checkout, we deploy and checkout the Optical Telescope Assembly (OTA), deploy the sunshade, extend the mast and rotate the OTA into its operational orientation. As the telescope cools down we perform the initial optics

alignments, checkout the instruments and begin instrument commissioning. Shortly after insertion in the L2 orbit, ≈ 4 months after launch, we begin science operations.
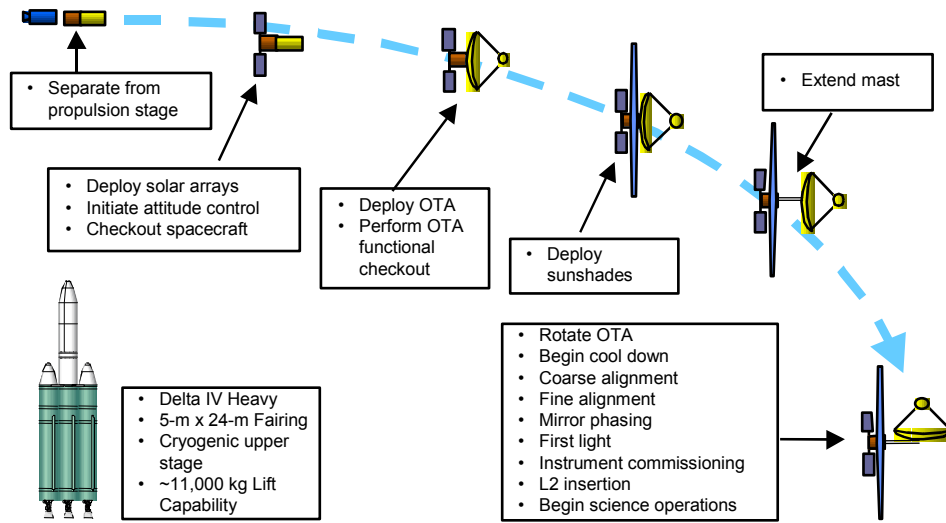
Figure 21. Launch and Commissioning Activities

2.1.1.5 Mission Operations

2.1.1.5.1 Command / control

Figure 22 shows the various elements of the TPF operations system, their main functions and the flow of data between them. We based our command and control approach for the Large Aperture IR Coronagraph (LAIRC) on the operations concept being developed for the Next Generation Space Telescope, with a Science Operations Center (SOC) to plan observations, and a Mission Operations Center (MOC) to generate the necessary commands and send them to spacecraft via a dedicated ≈ 10 m antenna. The MOC
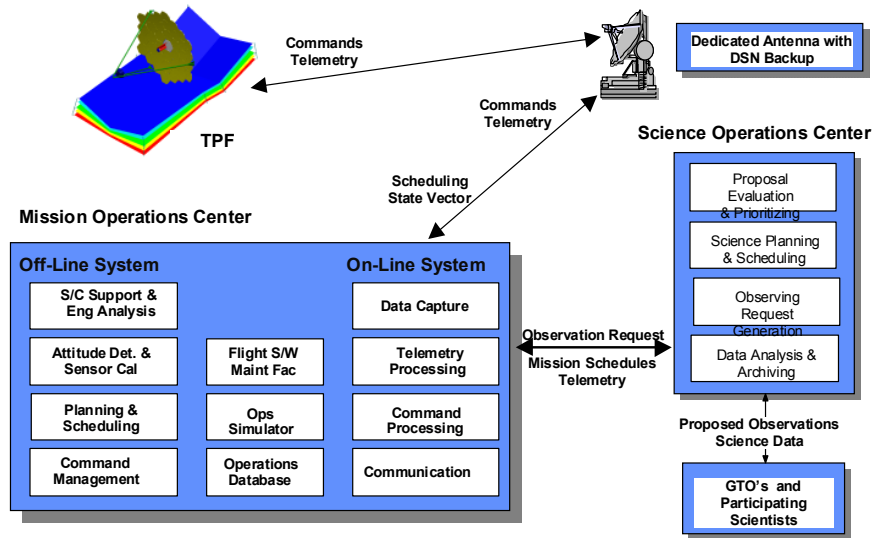
Figure 22. TPF Mission Operations Concept

also monitors the observatory state-of-health and retrieves and processes the downlinked data before forwarding it to the SOC for further processing, distribution to the science team, and archiving.

2.1.1.5.2   Calibration Sequences

Two major calibration activities will be performed using astronomical sources and / or internal calibration elements: (1) primary mirror segment and deformable mirror position updates, and (2) instrument radiometric and spectral calibrations.

Any point source of appropriate brightness can be used for calibration / verification of the primary mirror segment alignment and the deformable mirror (DM) settings. Our initial analysis of structural stability suggests that this process will need to be done approximately once per month after the initial commissioning of the telescope. We assume the primary mirror alignment process will be validated with NGST and/or a ground-based telescope such as Keck, and the DM adjustment process will be validated using the Eclipse testbed and other systems that use a DM. The data processing could be done using an automated on-board algorithm, but this is unlikely due to the large processing power required. More likely the required observations will be taken and the data sent to ground computers which will then calculate the required settings, which will then be uplinked to the spacecraft.

Instrument calibration requires pointing to standard astronomical sources. Internal calibration sources will also be needed for some instruments to provide data such as flat fields for the detectors, and spectral line calibrations for the spectrograph. The frequency of these calibrations will depend on the instrument configuration and detector quality. Considering the stability of existing instruments and the benign environment at L2, calibrations should not be required more than once a week, and once a month is more likely. The calibration data will be used to measure detector degradation, the effects of contamination on optical transmission, and long-term drifts in the detector readout electronics.

A typical calibration sequence would involve pointing the telescope to a bright standard star, acquiring it with the coronagraph, and making a series of observations using all available filters and occulting spot / Lyot mask pairs. The telescope will then be rolled ≈ 10 degrees about its optical axis and a second data set will be obtained. These data will be used to determine the PSF of the coronagraph images to allow PSF subtraction, at least for widely separated planet/star pairs. The telescope will then be pointed at a faint photometric standard star and images acquired in the viewable area of the coronagraph at locations where there is no obscuration of the star. Once again data are taken with all available filters and each occulting spot / Lyot mask pair. The flip mirror is then inserted into the beam and similar sets of data are obtained in the spectrograph. A complete set of observations should also be obtained with any other instruments that are included in the instrument suite. If the instrument is field split, they can be done simultaneously with the coronagraph instrument calibration sequences, provided power and data lines are not shared between the instruments.

Additional internal calibration sequences are required in addition to the photometric calibration provided by standard stars. Most important is a measure of the dark current that may be obtained by putting a dark slide in the filter wheel. Using a range of integration times similar to those of the observations, dark images are obtained. These can be taken while waiting for the telescope to settle after a slew and should be taken very frequently as they can be done with no impact to the observing efficiency. Also important is a flooded "flat field" image of each detector in the system. The detector needs to be uniformly illuminated to allow calibration of any pixel to pixel non-uniformity. This will also detect any pixels that go bad over the course of the mission. Since the detectors will degrade over time, this measurement is important. It may be possible to take these measurements during the settle time as well since they will not be taken through the large optics of the telescope, but limited to the instrument optics. Since the instrument structure is much stiffer than the telescope structure, the vibrations in the instrument should be damped very quickly after the target star is acquired. However, such measurements are only needed at most once per week, and perhaps only once per month so could be done only in conjunction with the photometric calibration.

2.1.1.5.3   Planet Detection Sequence

Planet detection sequences are fairly simple. First, the telescope is slewed to the target and vibrations are allowed to subside. The desired occulting spots, Lyot masks and filters are rotated into place with their respective wheels either during the slew or during the initial settling time. An occulting spot of 80 mas diameter is used for stars with a habitable zone (HZ) radius > 80 mas. Each spot has an optimized Lyot mask that is used with it. For a smaller HZ, a correspondingly smaller spot is used. In most cases, a 20% bandpass filter centered at 12 μm provides the maximum detectability for terrestrial planets. For small angular separations and/or for cooler primary stars, our performance models show filters centered at shorter wavelengths (10 or 11 μm) provide an equivalent SNR with a shorter integration time. Detailed modeling of the final instrument design should be done to determine the most advantageous observing mode for each target on the observing list while limiting the total number of observing modes to a few.

Target acquisition requires several steps, but the process is straightforward. The guide camera will acquire the target at the end of the slew and provide updates during the settling process to maintain pointing. Once the system has settled, the steering mirror in the telescope will center the target in the coronagraph's field of view using inputs from the guide camera. The guide camera will then acquire another guide star to provide guiding at the telescope level. The fine steering mirror in the coronagraph will then be used to center the target on the occulting spot and the observation will begin.

Integration times are limited to < 900 – 1000 seconds due to cosmic ray flux. Observations are split into at least two integration times, with more if needed. Using at least two integrations allows the telescope to roll from –5° to +5° around the line of sight to facilitate nearly exact subtraction of starlight from the image.

2.1.1.5.4 Planet Characterization Sequence

Once a planet has been detected, several observations must be taken using the detection sequence at several epochs to determine its orbit. If the planet is within the habitable zone, its spectrum must then be obtained to classify it. Since spectral observations are more difficult to obtain, they should be performed when the planet is near maximum elongation from the star.

The planet is acquired as for the detection mission, using the same occulting spot and Lyot mask. After acquisition with the coronagraph, the filter wheel inserts a 6 to 12 μm bandpass filter in the beam and the flip mirror directs the planet image to the spectrometer. At least two micro-shutters in the slit mask then open: one at the planet's position and one on the opposite side of the star. This allows fairly accurate star subtraction without needing to roll the observatory, provided the detector is well characterized. If additional sources are of interest in the same field, other slits may be opened, if they do not produce overlapping spectra.

Only 6–12 μm spectra will be obtained initially. If the spectrum indicates an atmosphere, additional data can be obtained in the 12 – 24 μm band by using the appropriate bandpass filter.

2.1.1.5.5 General Astrophysics operations

The operations for General Astrophysics (GA) are very similar to those for the planet detection and characterization missions. If the GA mission is performed using the coronagraphic instruments, the operations are identical. If they are done by field sharing a dedicated instrument, the only difference will be in the guiding mechanism. Unlike the detection mission, the GA imaging observations are likely to require multiple filter observations so changing the filter will need to be possible without introducing a large heat load that requires significant dissipation time. Some GA observations may be possible simply using the guide camera if the pointing can be done simultaneously (depends on the detector architecture). The observing mode flexibility will provide a large capability for doing a wide variety of GA observations.

2.1.1.6 "Day in the life"

Figure 23 shows a typical mission operations sequence for a two-month period during normal science operations. Scheduled activities include searching for planets around the target stars and follow-up observations for orbit determination and planet characterization; general astrophysics observations;

instrument and telescope calibration; and orbit maintenance maneuvers. Planet detection observations typically last a few hours to a few days, while characterization observations may last one to three weeks. We assume general astrophysics observing times will range from fractions of an hour to a day or more. We have dedicated ≈ 12 hours each month for instrument and telescope calibration/realignment and half a day every two months for stationkeeping maneuvers to maintain the halo orbit. During the 5 year design life of TPF we anticipate spending ≈ 375 days for planet detection, ≈ 565 days for planet characterization and ≈ 800 days observing general astrophysics targets. Another 72 days are allocated to slew and settle time, calibration and orbit maintenance, for an overall observing efficiency > 95%.
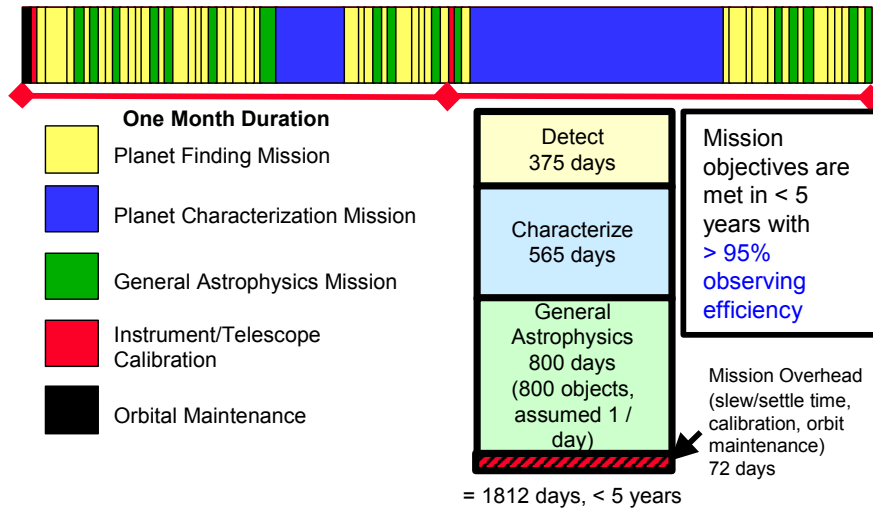
Figure 23. Typical Science Operations Sequence

2.1.2 Planet detection capabilities

2.1.2.1 Target Definition

For our Final Architecture Review (FAR) presentation, our primary target was the Earth 1 Au from the Sun located at a distance of 10 pc. We modeled the Sun and Earth as blackbodies of 5778 and 270 K respectively. The planet's flux was a combination of thermally emitted and reflected stellar light, assuming a 50% illumination factor. We included an endo-zodical light component using Marc Postman's model based on COBE data. The exo-zodi at the HZ of the exo-solar planet is estimated to be 2 times the endo-zodi contribution of a 45° view-angle as a representative case. This value is multiplied by the "zodi factor" to represent a variable zodiacal dust density that may be present in other star systems. We modeled other stellar systems in the same way using data on targets provided by Simon and Vogt for the Phase I study. This allowed us to compare our system's performance against a variety of stellar systems with different characteristics. Since the FAR our models have been updated to use the star, planet, and zodi spectral fluxes (for the Earth at 10pc) provided by the SWG.

2.1.2.2 Detection requirements

A source is considered "detected" if it is a point source, with at least an SNR of 5. It must also show the expected movement in the different epochs of observation given the target distance, approximate location of habitable zone, and proper motion. Outer planets can also be detected but should show the expected proper motion and possibly orbital motion if the orbital period is sufficiently short.

A detection is considered unambiguous if the source is detected in 2 of 3 observations at appropriate epochs to ensure that the source was not always within the inner radius probed by the observatory. We elected to go with 3 observations of each candidate system to maximize the probability of detection and minimize the probability of detecting a background source or other object not associated with the star system. We

increased the number of detection observations from 2 in Phase I to 3 to permit probing smaller HZ's with a reasonable probability of detection.

2.1.2.3 Capabilities

The LAIRC has significant capability to perform the detection portion of the TPF mission. Figure 24 shows the total observation time to detect the Earth at a variety of distances. As can be seen, the observation times are all quite reasonable, even for the small (67 mas) separation of the Earth at 15 pc.

Case	Integration Time Required	# Individual Observations	Time to execute 10 degree roll	Total Observation time
3 pc	< 30 seconds	2	1 hour	3630 seconds
5 pc	200 seconds	2	1 hour	4000 seconds
10 pc	3320 seconds	4	1 hour	7000 seconds
15 pc	60800 seconds	64	3 x 1 hour = 5 hours	71600 seconds ~20 hours

Figure 24. Time to Detect the Earth vs. Distance

All of these observations assume a 20% bandpass filter centered at 12 μm. We used a 60 mas diameter occulting spot for 15 pc case and a 80 mas diameter occulting spot for all of the other cases. The additional time allocated to roll the telescope is an estimate based on the spacecraft attitude control system design. The 3 and 5 pc case could easily be done without the roll, using a standard star PSF to remove the starlight since the SNR is very high at the large separations for those cases. This would greatly improve the overall observation efficiency. The approximately ≈ 2 hours to reposition the telescope to acquire the target is not included in this table.

2.1.2.4 Strengths/Weaknesses to target list

The target list provided by the SWG is very different from the target list generated by Simon and Vogt (S&V) in our Phase I study. The very small inner radius of the HZ (down to 30 mas) in the SWG list is not available to the LAIRC because of the large PSF of the central star. The list generated by (S&V) calculated a HZ based on an Earth analog. The inner radius of the HZ in that list is then approximately 70% of the calculated value. Their list of 162 stars had a minimum separation of 75 mas for the Earth analog, giving an inner HZ radius of approximately 52.5 mas. This is achievable with the LAIRC architecture. Therefore, we have elected to evaluate our architecture against the S&V list, rather than the target list provided by the SWG. The S&V list extends to much further distances and is biased towards brighter stars to achieve the required angular separations of the HZ. The corollary is that the LAIRC can probe the SWG list to approximately 50 mas but no further. The number of stars on the SWG list that have a minimum HZ of 50 mas or greater is only 87 which is just over ½ the required number of TPF targets.

Figure 25 shows the performance of our IR Coronagraph against a variety of stars on the Simon and Vogt list. They provide the stellar and planetary flux levels, calculated using a blackbody approximation. When the planetary values in their list for the Earth at 10pc are compared to the flux values provided by the SWG, they are somewhat lower, resulting in a longer required integration time. Therefore these integration time values can be taken as a worst case with the stellar systems in question needing further modeling to accurately calculate the planetary flux. Note that an increase of the zodiacal light contribution by a factor of 10 increases the integration time by less than a factor of 2 in the worst case (where the stellar flux is low) and does not affect the integration time for targets where the stellar flux is the dominant noise source.

Distance (pc)	Stellar Type	Angular separation (mas)	Integration time Case 1: 80 mas spot	Integration time Case 2: 60 mas spot	Integration time Case 3: 60 mas spot, separation reduced by 20 mas
12.1	G1	82	53 hours	21.9 hours	175 hours
26.2	F0	88	950 s	950 s	950 s
5.9	K4	79	25.6 hours	11.1 hours	106 hours
10.1	G6	89	1900 s	950 s	2850 s
16.2	F2	139	2850 s	2850 s	2850 s
17.4	G0	76	6.1 hours	2.1 hours	35.6 hours

| 21.4 | F5 | 101 | 2.4 hours | 2.4 hours | 3.96 hours |
| 22.7 | F7 | 80 | 10 hours | 4.75 hours | 38.8 hours |

Figure 25. Typical IR Coronagraph Planet Detection Integration Times

As shown, the primary weakness of the IR Coronagraph is the long integration times for faint planets at very small angular separations, which puts too much of the energy of the star at the planet location. It performs exceptionally well against targets with wider separations, brighter planets, and in the presence of increased zodiacal dust in the extra-solar system.

2.1.2.5 Characterization requirements

There are two parts to planet characterization: atmospheric characterization with low (R ≈ 20) resolution spectroscopy, and characterization of the planet's orbit and general photometric and astrometric parameters.

The 6-12 µm band includes the features of CH_4 (7.65 µm), CO_2 (9.31 and 10.42 µm), H_2O (7 µm), O_3 (9.65 µm) and N_2O (7.55 µm). We plan to make our initial spectroscopic observations in this band with a spectral resolution of 0.4 µm per pixel (R ≈ 19 at 7.5 µm) if sufficient signal can be obtained, and follow up with observations in the 12 – 24 µm band if warranted. Our spectrometer design has a plate scale of 0.1 µm per pixel, so 4 pixels will be binned to provide 0.4 µm resolution. This will be required for most targets to achieve the required SNR. The spectrometer's real spectral resolution is approximately 0.2 µm, so only 2 pixels will be binned (in the spectral direction) for bright targets to give the maximum spectral resolution. The goal is to obtain a SNR ≥ 5 for the lines of interest, which includes subtracting the continuum. Therefore, a SNR ≥ 7 must be obtained in the raw observation.

For astrometric orbital determination, a total of 7 observations are required. These observations can be the same as "detection" observations, since it is the location of the planet that is important. The timing of these observations is critical, though a null result is almost as useful as a positive result (provided there are not more than 2 in the data set) since the planet may, at times, orbit within the inner working distance if the inclination angle is sufficiently small. The spectroscopic observation(s) can be included in this data set, but the orbital elements should be known sufficiently well to allow the spectra to be obtained when the planet is near maximum angular separation from the star.

2.1.2.6 Capabilities

The LAIRC can take spectra of most targets it can detect. There is a limit when the planet gets close to the central star. Therefore, it is critical to take characterization measurements when the planet is at maximum separation from the star. Figure 26 lists the integration times required to achieve a SNR of 7 in the 9.5 µm blended line of CO_2 and O_3. The spectral resolution corresponds to an R ≈ 24. Also included is the time to reach SNR = 10 in the same line as a comparison. Obviously, for near and bright systems, a better SNR can be achieved in minimal time. This would be desirable to detect much fainter elements such as CH_4 and N_2O that are covered by our spectral band.

Case	Integration time to SNR = 7 @ > 9 µm	Integration time to SNR = 10 @ > 9 µm
3 pc	500 seconds	900 s
5 pc	1.85 hours	4.0 hours
10 pc	25.3 hours	51.2 hours
15 pc	625 hours (26 days)	1276 hours (53 days)

Figure 26: Characterization mission observing times

2.1.2.7 Astrophysics capabilities

Our IR Coronagraph, with its 28-m telescope, also has a significant capability for general astrophysics observations. With an angular resolution of 63 mas at 7 μm, a collecting area of $\approx$ 490 m^2, a 2.4 x 7.2 arc minute field-of-view, and an average mirror temperature of 21K, it is well suited for observations in 3 to $\approx$ 50 μm region. Since thermal radiation from the spacecraft is the dominant heat source, additional thermal shielding could lower the optics temperature into the 10-15K range.

Figure xx shows the sensitivity of our IR Coronagraph compared with that for other planned infrared observatories. The point source sensitivity in indicated for a 10^4 seconds integration time, a 20% bandpass ($\lambda/\Delta\lambda = 5$) and a 5-sigma detection. Both the 4-m and 8-m NGST telescopes and the 28-m TPF are assumed to have optics with an equilibrium temperature of 35K and an emissivity of 0.05. The zodiacal background limits the NGST and TPF sensitivity for $\lambda < 15\mu m$. One nanoJansky = 31.4 AB magnitudes. Also shown are the spectrum of a proto-galaxy that created 1 solar mass of new stars for 25Myr at Z = 3, 8 and 20, and the brightness of two of the faintest galaxies in the Hubble Deep Field at z $\approx$ 3 and z $\approx$ 4.

As shown below, TPF's point source sensitivity would be $\approx 10^2$ times greater than NGST, $\approx 10^4$ times greater than SIRTF, and 10^7 times greater than SOFIA. In particular, TPF could obtain a 5σ observation of a 25-day period Cepheid at J-band at 750 Mpc in $\approx$ 6 hours; measure IR surface brightness fluctuations at several gigaparsecs; get light curves and spectra of Type Ia supernovae at Z = 3; and image super starclusters at Z = 19 at an SNR of 10 in 6 hours; study disks and outflows around protostars and disks jets in active galactic nuclei; and obtain spectra of faint galaxies and other faint SIRTF and NGST discoveries.
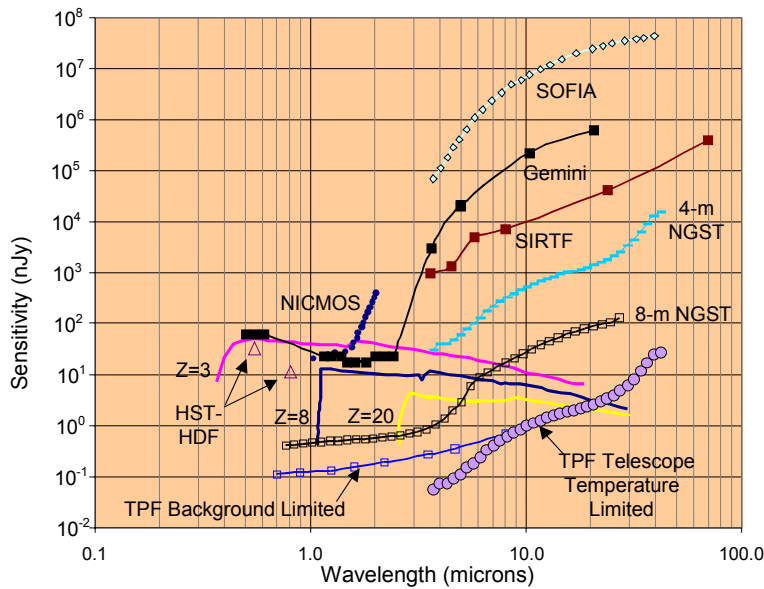
Figure xx. TPF Point Source Sensitivity Compared to Other Observatories

2.1.2.8 Origin Science targets and performance

Our Large Aperture IR Coronagraph is well suited for observations of science targets of interest to the Origins Program, including Proto-stars, debris disks and young Jovian Planets. It also has the ability to study cometary nuclei, Kuiper Belt objects and Brown dwarfs. Our telescope's resolution at (63 mas) is equal to that of the HST at 0.6 μm and it has $\approx$ 130 times more collecting area. Since the DM corrects the wave front errors within the 15 arcsecond field of view of the coronagraph to $\approx \lambda/60$ at 0.633 nm, a CCD (or HgCdTe) detector placed at the focal plane could achieve a resolution of $\approx$ 5.4 mas, nearly 12 times better than Hubble.

At the distance of Jupiter, this corresponds to a scale length of $\approx$ 16 km, $\approx$ 1800 times less than the size of the Great Red Spot, or $\approx$ 600 pixels across the disk of Ganymede. And the Large Aperture IR Coronagraph

will provide 10 times better angular resolution of the HH30 proto-stellar debris disk than the WFPC-2 image shown in Figure cc.

Figure cc. WFPC2 Image of HH30

Figure dd. Faint Galaxies Observed With HST

2.1.2.9 Galactic targets and performance

With a point source sensitivity 10^4 SIRTF the Large Aperture IR Coronagraph is well suited to follow-up the discoveries of SIRTF, SOFIA , NGST, and Herschel in the 3 to 50 μm wavelength region. This includes studies of molecular clouds, star formation, and circumstellar disks, Dwarfs and low mass stars, star clusters, evolved stars, planetary nebulae and the interstellar medium. We will be able to penetrate the cocoons of dust and molecular gas that surround proto-stars to study the debris disks within them as well as study the temperature, composition and physical process within the clouds. The 3-50 μm region is a rich spectral region with strong lines of water and molecular hydrogen, and many other species.
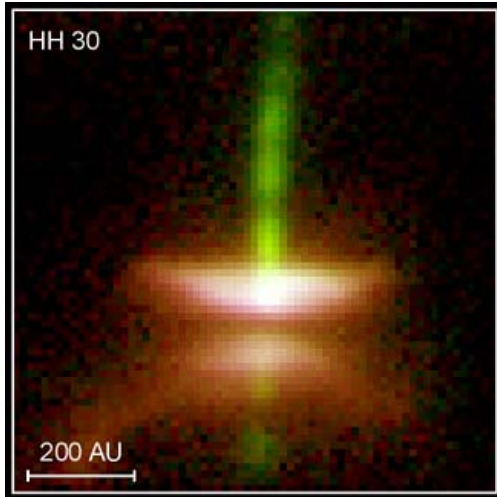
The large aperture IR Coronagraph will be sensitive to low surface brightness structures, which makes the detection and imaging of planetary debris disks such as the Vega or β Pic disks quite simple. And we can study stars 10x more distant or provide details on 10x finer scale than current space observatories. Our resolution (< 0.5 arcsec at 50 μm) will be ≈ 33 better than SIRTF and 8 times better than Herschel, and our coronagraphic capability will allow us to look deep within the protoplanetary disks of nearby stars.

2.1.2.10   Extragalactic targets and performance

The large aperture IR coronagraph will be able to conduct extensive imaging and spectroscopic studies of galaxies, ranging from the local neighborhood of our Milky Way Galaxy to the far reaches of the observable universe, including

- Ultraluminous Infrared Galaxies
- Active Galaxies / Active Galactic Nuclei
- Normal Galaxies and Starburst Galaxies
- Galaxy Clusters, and the
- ISM in External Galaxies

The unprecedented sensitivity and efficiency of the LAIRC will make it an ideal tool for conducting surveys of the extragalactic infrared sky. It could conduct a variety of mid-infrared imaging surveys. Deep, small-area surveys, including one centered on the Hubble Deep Field, could probe the early and Universe at redshifts >> 40. A three-color Deep Field image that took > 4 days to obtain with HST (Figure dd) would only take < 45 minutes of integration time with the LAIRC. Thus LAIRC would be an ideal tool to follow-up the observations of NGST, pushing back the boundaries of the observable universe even farther with observations of: the first luminous objects, early star and galaxy formation, the structure and dynamics of galaxies at z > 5, distant supernovae, Kuiper Belt objects and proto-planetary disks, and stellar populations in the nearby universe.

2.1.3 Mission feasibility

2.1.3.1 Technological needs

Figure yy lists the 'enabling' technologies for our IR Coronagraph, along with a number of 'enhancing' technologies that would significantly improve system performance and/or reduce the program cost. The key enabling technologies for our IR Coronagraph are large lightweight optics, high-contrast imaging technologies, large format Si:As detectors, large IR filters and broadband transmissive substrates. Enhancing technologies include lightweight suns-hades, low vibration cryocoolers, cryogenic mechanisms and wavefront sensing and control technologies.
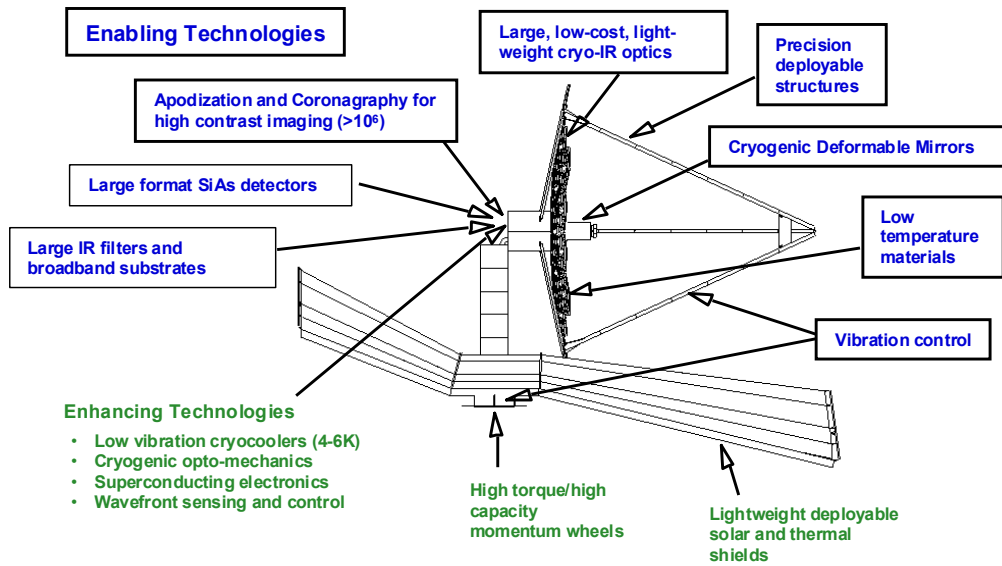
Figure yy. Key Technologies for the IR Coronagraph

2.1.3.2 Identification Of "Tall Tent Poles"

The most challenging ,"tall tent pole" technologies that that must be developed in order to build an IR Coronagraph are shown in Figure zz. Most of these technologies are already being developed for other missions such as NGST, but additional effort is required. Many other NASA programs require similar technologies, including FAIR, SPIRIT, SUVO, Life Finder and Planet Imager.

Technology	Current TRL	Development Risk	Being Developed By:
Large, lightweight Cryo-IR Optics	3	medium-high	**NGST***
Low cost mirror production	4	medium	**NGST***
Precision deployable structures	4	medium	**NGST***
Low temperature materials	2	medium	**NGST***
Active and passive isolators for vibration control	4	medium	**SIM***
Cryogenic Dampers	4	medium	
High contrast imaging (>10^6)	3	medium-high	**JPL-ETB**
Wavefront sensing and control	4	medium	**NGST***
Large format Si-As detectors	3	medium	**SIRTF***
Large IR filters & broadband transmissive substrates	2	medium-high	**SIRTF***
Low-vibration cryocoolers (4-6K)	4	medium	**TPF, Con-X**
Cryogenic opto-mechanisms	4	medium	**SIRTF***
Cryogenic deformable mirrors	4	Medium	**1 SBIR**
Lightweight, compact, nanometer resolution actuators	4	medium	**NGST***
Superconducting Electronics	3	medium	**BMDO***
Light-weight deployable solar & thermal shields	4	medium	**NGST***
High-torque/high capacity momentum wheels	3	medium-low	

"Tall Poles"　　　　　　*** Additional technology development effort required**

Figure zz. Critical "Tall Pole" Technologies

These technologies are currently at TRL 2 or 3. No breakthroughs are required to develop these technologies for TPF, however, only an extension of existing technologies given reasonable funding and a good engineering effort.

2.1.3.3　Current state of the art and technology development programs

2.1.3.3.1　Large, Lightweight Cryo-Optics

The 0.85-m beryllium mirror for SIRTF is diffraction limited at 6.5μm and has an areal density of ≈ 22 kg/m^2. The NGST mirror development program is developing glass and beryllium mirror segments with composite backing structures and cryogenic actuators that are DL at 2μm, with areal densities of ≈ 15 to 18 kg/m^2 and ≈ 17 kg/m^2, respectively.

In 1999 engineers at Composite Optics, Inc. (COI) manufactured a 2-m composite demonstrator mirror for the Herschel program by replication against a Cervit mold polished by the University of Arizona. This mirror had a surface accuracy of 2.32 μm rms. After removing the first 36 Zernickes, this mirror had a rms accuracy of 1.00 μm at room temperature and 1.21 μm at 30K. A 3.5-m mirror with this design would have an areal density of 11.4 kg/m^2.

On the East Coast, engineers at Composite Materials Associated (CMA) have been manufacturing composite membrane mirrors by replication against Pyrex molds for several years. They have produced a 15 cm spherical mirror with a 0.79 μm rms surface accuracy and 1.3 kg/m^2 areal density, and a 90 cm spherical mirror at 1.7 kg/m^2. Mid-spatial frequency errors < 3 nm RMS and a surface roughness < 10 Angstroms have also been demonstrated.

Our TPF design calls for lightweight, composite replica optics with an areal density of ≈ 5 kg/m^2 that are diffraction limited at 7 μm (3 μm goal), have mid-spatial frequency errors < 4 nm RMS, and a surface roughness < 100 Angstroms (30 Angstroms goal). We believe composite mirror technology is on track to meet these requirements by 2009.

A large, lightweight-optics technology development program for the IT Coronagraph should include:
- Low Temperature Resins Systems: Current designs are using EX-1515, a flight qualified cyanate ester with a 250F cure temperature. We need to investigate other resins (e.g., cyanate ciloxanes) to improve surface features, further reduce moisture effects and enhance toughness.
- Composite designs: Design and demonstrate quasi-isotropic layups, using the selected resin system, that provide the required CTE, CME, stiffness and strength.

- Mandrel production: Lower production costs through inexpensive metrology that leverages Bauer metrology or surface profilometry. Demonstrate segmented mandrel production and joining without discontinuity
- Large segment production: Demonstrate the required figure and control on large segments, and develop production plan to achieve 36 segments in 45 months

2.1.3.3.2   High Contrast ($> 10^{-6}$) Imaging

Solar coronagraphs observing the sun from the ground are can only observe coronal emission lines with a brightness of $\approx 10^{-4}$ times the brightness of the sun (B_{sun}), since the best skys are $\approx 10^{-4} B_{sun.}$ Space-based solar coronagraphs using multiple occulting disks in series, with subsequent disks removing diffraction from the previous disks, are able to observe the coronal continuum with scattered intensities of $\approx 10^{-6} B_{sun}$ an arcminute from the sun, and $\approx 10^{-10} B_{sun}$ a degree from the sun.

By comparison, coronagraphs designed to study the debris disks and search for planets around stars must operate at radial distances $<< 1$ arcsecond, and detect planets with brightness of $\approx 10^{-6} B_{star}$ in the infrared (≈ 10 μm) to $\approx 10^{-10} B_{star}$ in the visible (0.5 μm). Several HST instruments have used occulting spots to block the light from a central star. These instruments were not designed as coronagraphs, however, and have only been able to detect debris disk features with a brightness ≈ 50 times fainter than the scattered and diffracted starlight at that location.

The current state-of-the-art is represented by the Eclipse High Contrast Imaging Test Bed (Figure cc) that is currently under development at JPL.

The goal of the "Eclipse Testbed" (ETB) is to validate key wavefront and scattered light control technologies to the accuracy required to achieve 10^9 contrast ratios or better in visible light. It is being implemented as a vibration and temperature isolated vacuum testbed with reconfigurable optical setup (shown below) on a 7 x 5-foot optical bench.
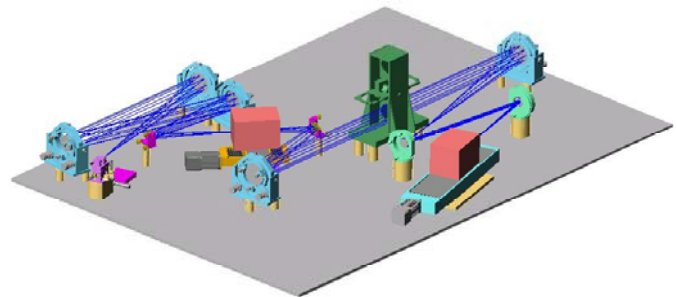
This program is funded by NASA/JPL, and is available to support the TPF program.

Figure cc. Eclipse Testbed

The ETB will be used to validate a number of key TPF coronagraph technologies. This includes demonstrating scattered light reduction with active optical wavefront correction to 1 Angstrom rms or better with a high-order precision deformable mirror, i.e.: a 1400 actuator DM in the Spring of 2002 and a 3200 actuator DM by Fall 2002. Diffracted light reduction with coronagraphic and apodizing techniques will also be demonstrated using "soft-edged" coronagraph occulting spots and a range of hard- and soft-edged Lyot/pupil stops.

Precision wavefront sensing techniques will be implemented with phase diversity algorithms using a CCD science camera moved through focus to provide the information needed to set active wavefront correcting elements including the DM and optics alignment actuators. High performance light baffling strategies will also be demonstrated.

The ETB data will enable us to validate our predictive models for an IR Coronagraph for TPF and for possible TPF precursor missions such as Eclipse. A precursor mission would minimize risk for TPF by validating our design approach, including the vibration isolation, thermal control and stray light control required to achieve the desired image quality. The Eclipse mission would also validate scaling our models from the testbed to a larger, operational system, and validate the wave front sensing and control algorithms in a space environment.

A precursor mission would be equally valuable for a preliminary survey of the TPF targets, enabling us to observe the exo-zodiacal dust/debris structures and densities and determine the integration times needed to overcome the zodiacal background. A precursor mission could also detect the giant planets that are the signposts for stable planetary systems and provide "safe harbors for terrestrial planets"

2.1.3.3.3   Large Format Si:As Detectors

Si:As detectors are considered critical for observing the Mid-IR wavelength range. Other detector technologies such as HgCdTe cannot reach beyond about 14 μm in area arrays and Si:Ga is not yet a mature technology, although development is continuing under the umbrella of such programs as NGST and SOFIA. Si:As detectors are mature, at least for ground-based astronomy, and can cover the entire 3 - 28 μm spectral wavelength range of our IR coronagraph. SIRTF is flying a number of Si:As detectors in formats up to 256 x 256 that will serve as the starting point for TPF detector technology development programs.

The goals of any detector technology development program for an IR Coronagraph for TPF should include:

- Larger formats. 512^2 and up to 1024^2 detectors are highly desirable for the TPF instruments to provide larger areal coverage. Some realizations of the instrument would greatly benefit from the largest formats possible (e.g. an Integral Field Unit).

- Lower dark current at higher temperatures. Long life cryo-coolers may not be able to provide the same temperatures as the LHe, which is used in SIRTF to achieve low dark current levels. Low dark current at 10 K operating temperature is highly desirable for the long integration times desired.

- Higher Quantum Efficiency. The $\approx 40\%$ QE now realizable is very low compared to other detectors. While difficult to improve, it provides very high leverage to the overall system performance.

- Lower Read Noise. For very low flux observations, read noise could become the limiting factor in the observation. While not applicable to the primary TPF mission of detecting and characterizing terrestrial planets, it will be needed for other Origins studies such as debris disk characterization.

2.1.3.3.4   Large Format IR Filters and Broadband Substrates

The substrates used in the coronagraph and spectrometer designs are all KCl. We chose this material because: (1) it is extremely transparent over the whole 3 to 28 μm band; (2) it has a very low refractive index (1.474 to 1.297); (3) it is available in large single crystals with extremely low scatter; and (4) as a single crystal material, it has intrinsically low refractive-index variations and no striae. For coronagraphs it is particularly important to avoid scatter from the occulting spot plane, since this light will appear in the final image. Thus we only considered materials that could be produced as single crystals. The low index may also be very important if we cannot AR coat the surface on which the occulting spot lies, since we could not tolerate the transmission loss that would result from an uncoated high-index surface. On the downside, KCl is not radiation hard, it is water soluble, and it is quite soft. The color centers produced by radiation damage are all in the visible ($\lambda < 825$ nm), however, and should not affect the IR performance. Although KCl and the other alkali halides are water soluble, they are not actually hydroscopic when very pure. Their hydroscopic behavior is due to the inclusion of a small amount of the corresponding alkali hydroxide, and Reactive Atmosphere Processed (RAP) alkali halides are free of the alkali hydroxide. Water can actually precipitate on pure KCl from 100% RH air and evaporate again without damage.

The substrates after the Lyot stop are not as critical. Here we would use high-index, radiation hard materials with better mechanical and chemical properties such as polycrystalline ZnSe and ZnS or single-crystal silicon and germanium. Except for hardness, slightly higher index and slightly greater vulnerability to grain pullout during manufacturing, ZnSe is optically superior in every way to all grades of ZnS. In addition, ZnSe is transparent over the 3 to 28 μm band, even at room temperature, while ZnS has a rather high absorption at the long end of the spectrum. ZnS is probably transparent enough at the longest wavelengths when cooled to ≈ 20 K; we need to obtain the low temperature optical constants to verify that. ZnSe is also very radiation hard and large pieces have been repeatedly been flown in space. Silicon is very attractive for its mechanical, thermal and optical properties except for its very high index. Since silicon and germanium (and diamond) are symmetric isoelectronic materials, their IR phonon absorption bands are strongly temperature dependent and essentially disappear at very low temperatures. There is little reason to use germanium in place of silicon because its index is so high and the band gap near 2.06 μm produces rather large dispersion at our shortest wavelengths. With its very high physical strength, silicon substrates can be extremely thin, although this advantage is offset somewhat by the presence of cleavage planes.

Our substrate choice downstream of the Lyot stop would probably be ZnSe, since filters on this material could be tested over their whole bandpass at room temperature. The filters required in the coronagraph and

spectrometer are not extremely large, but deposition uniformity will be an issue. Narrow-band filters in the 6 to 12 μm band should have minimum peak transmissions of 75% for 8% to 10% bandwidths. At longer wavelengths the minimum peak transmissions will be lower, dropping to 60% in the neighborhood of 14 μm, 55% around 15 μm and 40% at longer wavelengths. For wide-band filters (60% to 90% bandwidths) the minimum average transmission will be ≈ 75% below 5 μm, 80% from 5 to 11 μm, 70% around 12 μm, 65% from 13 to 14 μm, 55% at 15 μm and ≈ 40% beyond 16 μm.

Two technologies are beginning to improve filter performance: rugate and photonic filters. Rugate filters can sharpen and square off a filter, controlling its in-band ripple and out-of-band leakage. Some rugate filters are in commercial production (at least as special order items), but they may not provide much help in the deep IR where the major problem there is material absorption. Since our major goal for TPF is to increase peak transmission, rugate filter technology will probably not yield significant improvements, but this will have to be explored for cryogenic filters where the outlook could be somewhat better. Photonic filters are only in the very early stages of development, but one published result shows a very narrow-band filter with very good transmission and virtually no angular dependence on its center wavelength (although the bands do become wider at high angles of incidence). Photonic filter technology may have considerable applications to the IR because it makes the filter far less dependent on the intrinsic material properties.

2.1.4 Program Cost and Schedule

Our suggested schedule for the TPF Program is shown in Figure . The next 4 years of the TPF program will be devoted to technology development, precursor mission(s) development, and pre-phase A studies of two architecture classes leading to selection of a single architecture class in 2006. Two 24-month phase A studies initiated in 2007 will precede down-selection to a single prime contractor, followed by a 24-month Phase B and 48-month Phase C/D development effort. We currently envision launch in December 2014.

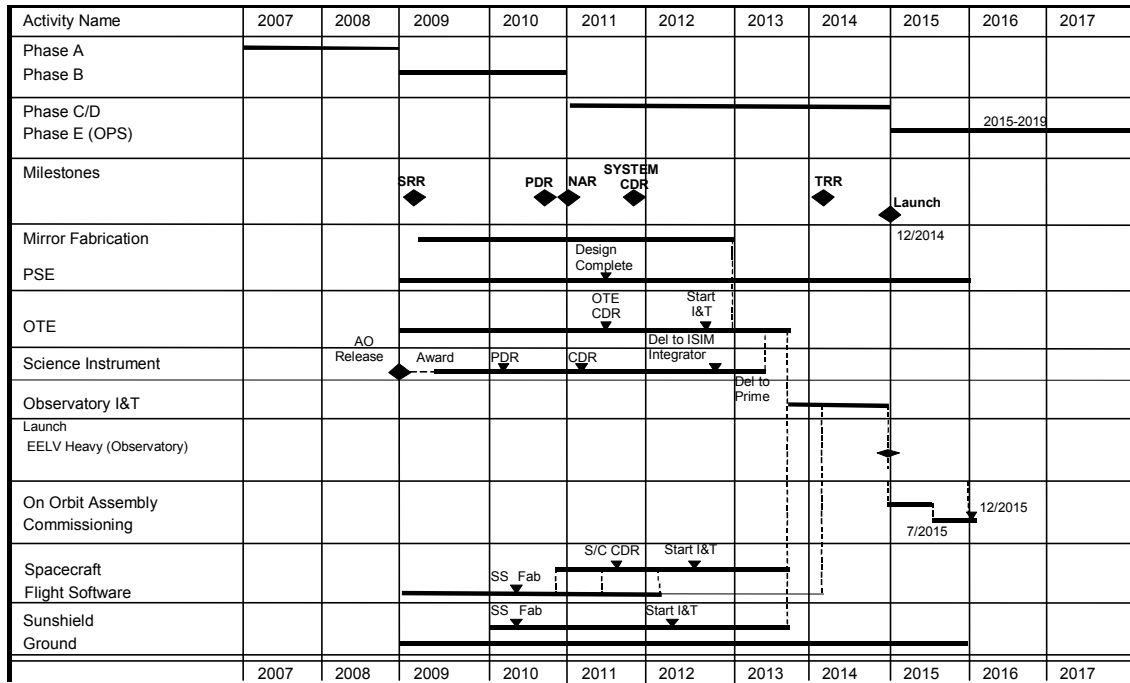| Activity Name	2007	2008	2009	2010	2011	2012	2013	2014	2015	2016	2017
Phase A											
Phase B											
Phase C/D											
Phase E (OPS)										2015-2019	
Milestones			SRR		PDR NAR	SYSTEM CDR		TRR	Launch 12/2014		
Mirror Fabrication				Design Complete							
PSE											
OTE		AO		OTE CDR	Start I&T Del to ISIM Integrator						
Science Instrument	Release	Award	PDR	CDR		Del to Prime					
Observatory I&T											
Launch EELV Heavy (Observatory)											
On Orbit Assembly Commissioning									7/2015	12/2015	
Spacecraft				S/C CDR	Start I&T						
Flight Software			SS Fab								
Sunshield			SS Fab	Start I&T							
Ground											
	2007	2008	2009	2010	2011	2012	2013	2014	2015	2016	2017

Figure . Program Schedule

At the TPF Final Architecture Review in December 2001 the four study contractors presented life cycle cost estimates that ranged from ≈ $1.2B to $1.9B in FY'02 dollars. Our point estimate for the Life Cycle Cost of an IR coronagraph, including $20M for Phase A studies and $50M for technology is $1.53B in FY'02 dollars. Figure shows a breakdown of our estimated costs, after adding a 30% reserve, from 2007 through the end of mission in 2024. [Annual science operations costs and support from NASA centers is not included]. Figure shows the funding required by program year, assuming constant operations costs of $10M per year from 2015 to 2024.

WBS	Description	Total 2002$M
	TPF Total	1896
1.0	Program Management	54
2.0	System Engineering	88
3.0	Assembly,Integration & Test	342
4.0	Spacecraft	339
5.0	Optical Telescope Element	623
6.0	Science Instruments	275
7.0	Mission Ops & Data Analysis	175

Figure . TPF Life Cycle Cost

	2007	2008	2009	2010	2011	2012	2013	2014	2015
Total Cost/Year	31.5	39.3	193.3	352.2	379.4	384.9	272.4	145.5	10

Figure . Funding Profile

2.1.5 Summary

Our study indicates the IR Coronagraph we designed during Phase II meets the TPF mission requirements and has the greatest general astrophysics capabilities of all of the architectures that we examined, including interferometers, sparse apertures, Fresnel telescopes and free flying occultors.

During the course of this Mission Architecture study our TRW team performed objective trades on five different architecture classes applicable to TPF mission (and found all of the concepts are very challenging). We normalized planet detection/characterization across all of these architectures and assessed them using the JPL evaluation criteria of technology maturity, cost, risk, reliability/robustness, astrophysics capability, and legacy. All of the architectures fell into two classes: Direct Imagers that provide simultaneous coverage of u-v plane (telescopes) and Synthetic Imagers that provide sequential coverage of u-v plane (interferometers).

We found Direct Imagers have advantages over Synthetic Imagers, given normalized detection/characterization performance, since:

- Direct Imagers have more science utility than synthetic aperture imagers, since they are less subject to confusion, handle extended objects better, readily support spectroscopy and have the flexibility to respond to the unexpected;

- Direct imagers are less complex to implement, and do not require beam transport over long distances, array rotation or chopping, or precision pathlength control;

- Direct imaging and IR Coronagraphy will require less technology development, thanks to heritage from SIRTF, SIM and NGST and the coronagraph technology being developed at JPL with the Eclipse testbed; and

- Direct imagers can be scaled directly to the LifeFinder and Planet Imager missions.

We concluded that the TPF mission is technically feasible, provided enabling technologies are developed in the 2002-2009 period. No technology "breakthroughs" required, only an extension of current state-of-the-art; and many missions enabled by TPF technology development

Our cost estimate suggests the TPF mission can be accomplished for a Life Cycle Cost of ≈ $1,900M in FY02 dollars and we believe TPF could be launched in late 2014 if our recommended schedule (with PDR in late-2010 and CDR in late-2011) is adopted.

2.1.6 Acknowledgements

We thank our Science Team members and Industry Partners for their support, and Dr. John Trauger for his Performance Model Calculations. Figure aa lists the members of our TPF Study Team, and Figure bb lists the individuals who contributed to the Phase II study effort. This work was performed under JPL Contract No. 1217284.

Team Member	Role
• Science Team	Phenomenology, concepts, astrophysics, concept assessments
• TRW	Prime, system engineering, spacecraft
• Bauer	System performance modeling
• Kodak	Optical technology
• ITT	Modeling, instrument technology
• LLNL	Modeling, instrument technology
• SEE	Orbit analysis
• SDL	Instrument technology

Figure aa. TRW Study Team Members

Industry		Industry	
Name	**Company/Role**	Name	Company/Role
Charlie Atkinson	TRW Optics, I&T	Bob Robitaille	TRW Pricing
Suzi Casement	TRW Science Instrument	Ken Sitarski	TRW Subcontracts
Sherry Erdman	TRW Secretary	Maraia Tanner	TRW Mechanical Design
Marty Flannery	TRW Optical Design	Frank Tung	TRW Attitude Control
Paul Glenn	Bauer Performance Model	Ed Wood	West Winds Cost Analysis
John Kinney	TRW Data System	**Science Team**	
Keith Kroening	TRW Spacecraft, MDI	**Name**	**Organization**
Chuck Lillie	TRW Program Manager	Alan Dressler	Carnegie Observatories
Ray Manning	TRW Dynamics	James Larkin	UCLA
Gary Matthews	Kodak Optics Support	Doug Lin	Lick Observatory
Leo Matuszak	TRW Launch Vehicles	Richard Simon	NAAO
Stewart Moses	TRW System Engineer	Glenn Starkman	Case Western Reserve Univ.
Tammy Ortiz	TRW Contracts	John Trauger	JPL
Annette Palazuelos	TRW Business	Dan Weedman	Self
John Pohner	TRW Thermal Analysis	Ned Wright	UCLA

Figure bb. TPF Phase II Study Contributors